Coordinated Path-Following Control of Fixed-Wing Unmanned Aerial Vehicles

Hao Chen, Yirui Cong, *Member, IEEE*, Xiangke Wang, *Senior Member, IEEE*
Xin Xu, *Senior Member, IEEE*, and Lincheng Shen

***Abstract*—This article investigates the problem of coordinated path following for fixed-wing unmanned aerial vehicles (UAVs) with speed constraints in the two-dimensional plane. The objective is to steer a fleet of UAVs along the path(s) while achieving the desired sequenced inter-UAV arc distance. In contrast to the previous coordinated path-following studies, we are able through our proposed hybrid control law to deal with the forward speed and the angular speed constraints of fixed-wing UAVs. More specifically, the hybrid control law makes all the UAVs work at two different levels: 1) those UAVs whose path-following errors are within an invariant set (i.e., the designed coordination set) work at the coordination level and 2) the other UAVs work at the single-agent level. At the coordination level, we prove that even with speed constraints, the proposed control law can make sure the path-following errors reduce to zero, while the inter-UAV arc distances converge to the desired value. At the single-agent level, analysis for the path-following error entering the coordination set is provided. We develop a hardware-in-the-loop simulation testbed of the multi-UAV system by using actual autopilots and the X-Plane simulator. The effectiveness of the proposed approach is corroborated with both numerical simulation and the testbed.**

***Index Terms*—Coordinated path following, hybrid control, multiunmanned aerial vehicle (UAV) systems, speed constraints.**

I. Introduction

A. Motivation

COORDINATED path-following control of multiple fixed-wing unmanned aerial vehicles (UAVs) has attracted significant attention in recent years, due to its increasing demands in civil and military uses [1]. It studies how to steer a group of fixed-wing UAVs moving along given/planned paths while forming a desired formation pattern based on local interactions.

Different from multirotor UAVs or ground vehicles, a fixed-wing UAV cannot move backward and is actually constrained by a minimum forward speed to generate sufficient lift to support itself in flight. With the minimum forward speed constraint, the coordinated path-following control behaves very differently.

1) During path following, the maximum angular speed is not negligible any more, since it combined with the minimum forward speed determines the minimum turning radius. As a result, one UAV can only follow the class of paths (curves) with limited curvature, which is determined by the minimum forward speed and the maximum angular speed; while the existing studies in the coordinated path-following control problems did not take the speed-related curvature into account.
2) During the formation pattern forming process, one UAV cannot completely stop or become unacceptably slow to wait for another UAV. Consequently, some coordinating UAVs can quit the group formation, if the minimum forward speed and the maximum angular speed are not properly considered when designing the control law.

Therefore, the coordinated path-following control of fixed-wing UAVs is very different from that without minimum forward speed and maximum angular speed constraints in the literature, and cannot be solved by the existing methods (e.g., [2]). It is necessary to design an efficient control law to solve the coordinated path-following control problem for fixed-wing UAVs.

B. Related Work

Fixed-wing UAVs are typical nonholonomic systems. As indicated in [3], the relative difficulty of their control problems depends not only on the system's nonholonomic nature but also on the control objective. There are two objectives corresponding to the coordinated path-following control problem, i.e., path following and multivehicle coordination.

The path-following problem has a long history dating back to the last century [4]. For fixed-wing UAV path following, some early work mainly focused on following straight lines, circles, or their combinations [5]–[7]. A comparison of existing methods dealing with these path-following problems can be found in [8]. In recent years, general curved path-following problem has received increasing attention, and typical approaches include pursuit-based guidance method [9], [10], proportional–integral–derivative (PID) control [11], vector field method [12], [13], sliding-mode control [14], backstepping control [15], adaptive control [16], nested saturation and control Lyapunov function-based method [17], etc.

Manuscript received May 11, 2020; revised November 7, 2020; accepted December 29, 2020. This work was supported by the National Natural Science Foundation of China under Grant 61973309, Grant 61801494, and Grant 61825305. This article was recommended by Associate Editor C.-C. Lim. *(Corresponding author: Xiangke Wang.)*

The authors are with the College of Intelligence Science and Technology, National University of Defense Technology, Changsha 410073, China (e-mail: xkwang@nudt.edu.cn).

Color versions of one or more figures in this article are available at https://doi.org/10.1109/TSMC.2021.3049681.
Digital Object Identifier 10.1109/TSMC.2021.3049681

In terms of the multivehicle coordination, typical methods include the leader–follower approach [18]–[20], virtual structure approach [21]–[23], and behavior-based approach [24], [25]. We recommend the surveys in [26] and [27] to readers who are interested in the existing coordinated control results. Some methods have been validated by the formation flight of fixed-wing UAVs: in [28], a vision-aided close formation flight of two UAVs was conducted based on leader–follower control; the work in [29] considered several formation design approaches, and performed field experiments of two UAVs with a combined controller; as a big advance in terms of the scale, the autonomous flight of 50 fixed-wing platforms was presented in [30], but details of their control law were not provided.

To combine the path-following controller with the coordinated control architecture is the key factor to achieve coordinated path following. There are a large number of studies dealing with the coordinated path-following control of multirotor UAVs [31] and ground vehicles [21], [32]. However, most of these results cannot be applied to fixed-wing UAVs, since they are constrained by the minimum forward speed, which is a hard constraint in this kind of vehicle for certain missions. The speed constraints have been partially considered in the coordinated path-following problems for fixed-wing UAVs: in [33], a time-critical coordinated path-following control law was proposed to steer a fleet of fixed-wing UAVs along given paths while arriving at their own destinations simultaneously, but only the forward speed constraints are considered and the angular speed commands are assumed not to lead to saturation; the cooperative moving path-following problem was introduced in [34], with sufficient conditions derived for asymptotic stability, but the angular speed constraints are only guaranteed to be satisfied at steady states. Besides, in [33] and [34], they did not consider what if the sufficient conditions for the convergence of coordinated path-following error are not satisfied under their control laws.

C. Our Contributions

In this work, we focus on the coordinated path-following control of fixed-wing UAVs. Considering the speed constraints of fixed-wing UAVs, we propose a novel distributed hybrid control approach. The main contributions are listed as follows.

1) We propose a hybrid control framework based on an invariant set, the *coordination set*, to solve the coordinated path-following problem of fixed-wing UAVs. Different from the existing results, the coordination set is designed to guarantee the convergence of the path-following error and coordination error while satisfying both the forward speed constraints and the angular speed constraints.
2) We propose the coordinated path-following control law inside the coordination set, and theoretically prove that even with the speed constraints of fixed-wing UAVs, the proposed control law can make the path-following errors reduce to zero, while the inter-UAV arc distances converge to the desired value.
3) We propose the single-agent level control law outside the coordination set by using optimal control, and the convergence analysis for the UAVs entering the coordination set is provided.
4) We develop a hardware-in-the-loop (HIL) simulation testbed of the multi-UAV system by using actual autopilots and the X-Plane simulator, and validate the proposed coordinated path-following approach with the testbed.

D. Article Organization

This article is organized as follows. Section II presents the system model as well as the problem description and analyzes the difficulty from speed constraints. Then, in the next two sections, we present our control law to tackle the coordinated path-following problem with speed constraints: at the coordination level when the path-following error is within a coordination set (see Section III); and at the single-agent level when it is outside this coordination set (see Section IV). In Section V, we show the simulation results, including numerical simulation and the HIL simulation, with the X-Plane simulator; and finally, the concluding remarks are given in Section VI.

E. Notation

A curve is said to be $\mathcal{C}^k$-smooth, if it admits an analytic expression $\Gamma(x, y)$, whose kth derivative exists and is continuous. The curvature of a path at point p on the curve is denoted as $\kappa(p)$. $\mathbf{T}(p)$ denotes the unit tangent vector of the curve at p, and the curvature at p is defined as $\kappa(p) = \mathrm{d}\mathbf{T}(p)/\mathrm{d}s$, where s is the natural parameter representing the curve length.

II. Coordinated Path-Following Problem for Fixed-Wing UAVs

In this section, we formulate the two-dimensional coordinated path-following problem for a group of n homogeneous fixed-wing UAVs. The aim is to design a control law such that each UAV follows a predefined curved path while the sequenced inter-UAV arc distances converge to the desired constant.

A. System Model and Problem Description

Consider a group of fixed-wing UAVs flying at the same altitude. Then, the state of the ith UAV can be represented by the configuration vector $q_i = (x_i, y_i, \theta_i)^T \in \mathbb{R}^2 \times [-\pi, \pi)$, where (x_i, y_i) is the ith UAV's position defined in an inertia coordinate frame $\mathcal{W}$, and θ_i is the orientation of the ith UAV with respect to the x-axis of $\mathcal{W}$. The motion of a fixed-wing UAV can be described by a fairly complicated set of 12 nonlinear, coupled, first-order, ordinary differential equations [35]. However, when a UAV is moving on a plane, its kinematic model can be written as follows [5], [8], [13]:

$$\begin{cases} \dot{x}_i = v_i \cos\theta_i \\ \dot{y}_i = v_i \sin\theta_i \\ \dot{\theta}_i = \omega_i \end{cases} \tag{1}$$

where the control inputs v_i and ω_i stand for the forward speed and angular speed of the ith UAV, respectively.

For fixed-wing UAVs, the speed constraints must be considered. On the one hand, the forward speed of a UAV is

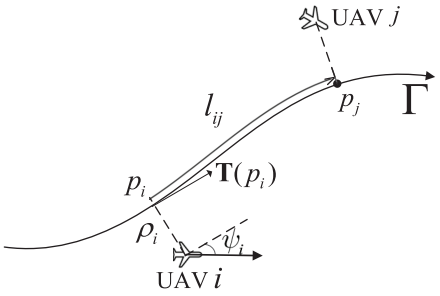

Fig. 1. Path Γ with a direction. Points p_i and p_j are the projections of the ith and the jth UAVs, respectively. $\phi_i = (\rho_i, \psi_i)$ is the path-following error of the ith UAV, and arc distance l_{ij} is the length along the path from p_i to p_j. In this case, the jth UAV is the preneighbor of the ith UAV.

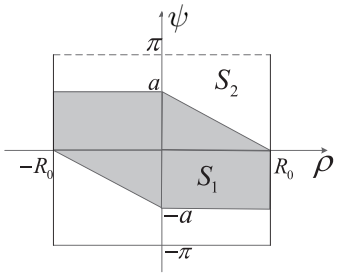

Fig. 2. Set $\mathcal{S}$ with its two partitioned subsets $\mathcal{S}_1$ and $\mathcal{S}_2$ in [2].

constrained with saturation and dead zone, i.e., each fixed-wing UAV has the maximum and minimum forward speed constraints. On the other hand, the angular speed is constrained with saturation. Mathematically, the constraints are

$$\begin{cases} 0 < v_{\min} \le v_i \le v_{\max} \\ |\omega_i| \le \omega_{\max} \end{cases} \tag{2}$$

where $v_{\min}$ and $v_{\max}$ are the minimum and maximum forward speeds, while $\omega_{\max}$ is the maximum angular speed. We consider all the UAVs follow a directed curved path $\Gamma \in \mathcal{C}^2$. As indicated in [36], the path-following error and the coordination error can be analyzed separately. We present them one by one.

Assumption 1: Γ is globally known to each UAV, and the absolute value of the curvature of Γ at any point p is less than a constant κ_0, i.e., $|\kappa(p)| < \kappa_0$.

Due to the speed constraints of a fixed-wing UAV, κ_0 must be no larger than $\omega_{\max}/v_{\min}$, i.e., each UAV has a minimum turning radius (numerically equals $v_{\min}/\omega_{\max}$) when following a path. We use $\mathbf{T}(p)$ to denote the tangent vector of the path Γ at point $p = (p_x, p_y)^T$, and point p is said to be a projection of the ith UAV, if the vector $\boldsymbol{t} = (x_i - p_x, y_i - p_y)^T$ is orthogonal to $\mathbf{T}(p)$. We define $\phi_i = (\rho_i, \psi_i)$ as the path-following error of the ith UAV with respect to the path Γ (see Fig. 1), where $\rho_i \in \mathbb{R}$ is the distance from the ith UAV to its closest projection p_i on Γ with a sign: $\rho_i > 0$ when the ith UAV is on the left-hand side of Γ in the direction of the path, and $\rho_i < 0$ when it is on the other side. For example, in Fig. 1, we have $\rho_i < 0$ and $\rho_j > 0$. ψ_i is the heading of the ith UAV with respect to $\mathbf{T}(p_i)$ at its projection p_i. In this way, ρ_i can be seen as the *location difference* of the ith UAV with respect to the path Γ; and $\psi_i \in [-\pi, \pi)$ is the *orientation difference* between the heading of the ith UAV and $\mathbf{T}(p_i)$.

Remark 1: If $|\rho_i| < R_0$, where $R_0 = (1/\kappa_0)$, the closest projection p_i is unique [4].

The dynamics (1) thus can be rewritten in the form of $\dot{\phi}_i = f(\phi_i)$ with the speed constraints represented by (2)

$$\begin{cases} \dot{\rho}_i = v_i \sin\psi_i \\ \dot{\psi}_i = \omega_i - \frac{\kappa(p_i) v_i \cos\psi_i}{1-\kappa(p_i)\rho_i}, \end{cases} \quad i = 1, \ldots, n. \tag{3}$$

UAV i asymptotically follows the path Γ if and only if $\phi_i \to \mathbf{0}$.

In our coordinated path-following problem, it not only requires all the UAVs to move along the path Γ but also guarantees the distance between any two adjacent UAVs is a desired constant L in the sense of the arc length. To describe adjacent UAVs, we introduce the following definition.

Definition 1: The jth UAV is the ith UAV's *preneighbor* if:

1) $|\rho_i| < R_0$, $|\rho_j| < R_0$;
2) the projection point p_j of the jth UAV on the path Γ is in front of the ith UAV's projection point p_i (see Fig. 1), without any other UAV's projection in the middle.

The two conditions in Definition 1 imply that: 1) the preneighbor definition only works for the UAVs close enough to the path Γ (i.e., with $|\rho_i| < R_0$) and 2) each UAV can at most have one preneighbor.

Remark 2: When there are two or more UAVs with the same projection point on Γ, we define the preneighbor in ascending order with respect to the UAVs' labels to avoid ambiguity.

Since the desired inter-UAV arc distance is between adjacent UAVs, the ith UAV just needs to focus on the arc distance l_{ij} to its preneighbor. To simplify the description, we denote the arc distance between the ith UAV and its preneighbor as ζ_i. The coordination error for the ith UAV is thus $L - \zeta_i$.

Now, we can formally define the coordinated path-following problem for fixed-wing UAVs as follows.

Problem 1 (Coordinated Path Following): Given n fixed-wing UAVs, each is modeled as (1) with speed constraints represented by (2), the design control law such that $\phi_i \to \mathbf{0}$, and $L - \zeta_i \to 0$, $i = 1, \ldots, n$,

B. Challenge From Speed Constraints

When ignoring the speed constraints, we can extract a set $\mathcal{S}$ as $\mathcal{S} = \{(\rho, \psi) : \rho \in [-R_0, R_0], \psi \in [-\pi, \pi)\}$, which is illustrated in Fig. 2, as defined in [2], where $\mathcal{S}$ is partitioned into two parts $\mathcal{S}_1$ and $\mathcal{S}_2$. $\mathcal{S}_1$ is the coordination set, defined as $\mathcal{S}_1 := \{(\rho, \psi) \in \mathcal{S} : |\rho| \le R_0, |\psi| \le a, |a\rho + R_0\psi| \le aR_0\}$, and $\mathcal{S}_2 := \mathcal{S} \setminus \mathcal{S}_1$. Parameter a satisfies $0 < a < \min\{(\pi/2), R_0\}$.

It has been proved that by applying an appropriate hybrid control law, the path-following error ϕ_i of the ith UAV, whose dynamics are represented by (3) without constraints represented by (2), converges to $\mathbf{0}$. To be more specific, if ϕ_i is in $\mathcal{S}_2$ initially, then it cannot leave $\mathcal{S}$ and will enter $\mathcal{S}_1$ in a finite time, and finally converge to $\mathbf{0}$, with the arc distance ζ_i approaching L as $t \to \infty$. In this process, when $\phi_i(t) \in \mathcal{S}_2$, the ith UAV only works at a single-agent level (i.e., without any coordination), and the coordination algorithm gets to

work only after ϕ_i gets into the coordination set. Unfortunately, when considering the speed constraints represented by (2), the above results cannot be guaranteed.

Remark 3: We can always characterize a small region $\mathcal{S}_e$, such that when $\phi_i(t_0) \in \mathcal{S}_e$, given any control input $(v_i, \omega_i) \in [v_{\min}, v_{\max}] \times [-\omega_{\max}, \omega_{\max}]$, there exists a time $t_1 > t_0$ such that $\phi_i(t_1) \notin \mathcal{S}$. Without loss of generality, we assume the UAVs follow a path with the curvature $\kappa(p_i) \in (-\kappa_0, 0]$. We define $\mathcal{S}_e = \{\phi_i \in \mathcal{S} : [(v_{\min}(\psi_i - \epsilon_0)\sin\epsilon_0)/\omega_{\max}] + \rho_i - R_0 > 0,\ \rho_i \in [0, R_0], \psi_i \in [0, \pi/2]\}$, where $0 < \epsilon_0 < \pi/2$. We note that $\mathcal{S}_e$ is not an empty set; otherwise, $[(v_{\min}(\psi_i - \epsilon_0)\sin\epsilon_0)/\omega_{\max}] + \rho_i - R_0 \le 0$ should hold for all $\rho_i \in [0, R_0]$ and $\psi_i \in [0, \pi/2]$, which can be verified to be impossible by taking $\rho_i = R_0$ and $\psi_i = \pi/2$. According to (3), when $\psi_i \in [\epsilon_0, \pi/2]$, $\dot{\psi}_i = \omega_i - [(\kappa(p_i)v_i\cos\psi_i)/(1-\kappa(p_i)\rho_i)] \ge -\omega_{\max}$. Suppose t^* is the minimum time it takes to satisfy $\psi_i \le \epsilon_0$, then $t^* \ge [(\psi_i(t_0) - \epsilon_0)/\omega_{\max}]$. When $t \in [t_0, t_0 + t^*]$, we have $\dot{\rho}_i = v_i \sin\psi_i \ge v_{\min}\sin\epsilon_0 > 0$ and, thus, $\dot{\rho}_i \cdot [(\psi_i(t_0) - \epsilon_0)/\omega_{\max}] \ge [(v_{\min}(\psi_i(t_0) - \epsilon_0)\sin\epsilon_0)/\omega_{\max}] > R_0 - \rho_i(t_0)$, meaning ϕ_i will leave $\mathcal{S}$ before $t_0 + t^*$. Therefore, it is impossible to use the results in [2] to solve the speed-constrained coordinated path-following problem defined in Problem 1, since not all the points in $\mathcal{S}$ can be guaranteed always within $\mathcal{S}$ even under any possible control input.

To solve Problem 1, we have to further partition set $\mathcal{S}$ to specify the invariant subsets and design the control laws accordingly. To be more specific, we define a new coordination set and propose the corresponding control law in Section III; and for the points outside the coordination set, we design a single-agent level control law in Section IV.

Before we proceed, the following lemma is necessary throughout this article.

Lemma 1 [37, pp. 61–62]: Consider a simple closed contour defined by $g(x) = 0$, with $g(x) < 0$ enclosed by the contour, where $g(x)$ is a continuously differentiable function. The vector field $f(x)$ at a point x on the contour points inward if the inner product of $f(x)$ and the gradient vector $\nabla g(x)$ is negative, i.e., $f(x) \cdot \nabla g(x) < 0$; and the vector field points outward if $f(x) \cdot \nabla g(x) > 0$; and it is tangent to the contour if $f(x) \cdot \nabla g(x) = 0$. The trajectory can leave the set enclosed by the contour, only if the vector field points outward at some point on its boundary, i.e., $\exists\ x$ such that $g(x) = 0$ and $f(x) \cdot \nabla g(x) > 0$.

III. Coordinated Control Law in Coordination Set

In this section, we discuss how to control the UAVs, whose path-following errors are within a given set (called the coordination set $\mathcal{S}_1$), to move along the path Γ in a coordination manner.

We formulate the coordination set as $\mathcal{S}_1 = \{(\rho, \psi) : |\rho| \le R_1, |\psi| \le a, |a\rho + R_1\psi| \le aR_1\}$, where $R_1 < R_0$. Since $\kappa_0 = (1/R_0)$, we have $\kappa_0 R_1 < 1$. We note that this newly defined coordination set is relatively smaller compared to that without considering the speed constraints (see Fig. 2). With speed constraints, parameters a and R_1 should be properly selected. Thus, we first illustrate the parameter selection (Section III-A) before designing the control law (Section III-B).

A. Parameter Selection of $\mathcal{S}_1$

The selection of parameters in $\mathcal{S}_1$ follows two basic principles, which are illustrated one by one as follows.

1) First Principle: We need to guarantee the existence of a proper control law making $\mathcal{S}_1$ an *invariant set* (see [37, p. 127]), i.e., if the initial path-following error $\phi_i(t_0) \in \mathcal{S}_1$ at time t_0, then $\phi_i(t) \in \mathcal{S}_1$ for any $t > t_0$. In that way, for each $\phi_i(t_0) \notin \mathcal{S}_1$, we only need to design the control law to guarantee $\phi_i(t)$ entering $\mathcal{S}_1$.

Remark 4: Denote the set $\partial\mathcal{S}_1$, as the intersection of $\mathcal{S}_1$ with the following set: $\{(\rho, \psi) : |\psi| = a\} \cup \{(\rho, \psi) : |a\rho + R_1\psi| = aR_1\}$. It can be seen that $\partial\mathcal{S}_1$ is a subset of the boundary of $\mathcal{S}_1$. According to Lemma 1, the first principle to guarantee $\phi_i(t)$ will not leave $\mathcal{S}_1$ is equivalent to guarantee $\phi_i(t)$ will never get across $|a\rho + R_1\psi| = aR_1$ in the first and the third quadrants, and $|\psi| = a$ in the second and fourth quadrants. Since $v_i > 0$, it is certain that $\phi_i(t)$ will never leave $\mathcal{S}_1$ from $|\rho| = R_1$ in the second and the fourth quadrants, and that is why we do not include set $\{(\rho, \psi) : |\rho| = R_1\}$ in $\partial\mathcal{S}_1$.

Then, we have the following lemma.

Lemma 2: A sufficient condition under the first principle is that, for any $\phi_i \in \partial\mathcal{S}_1$, there exist v_i and ω_i satisfying (2), such that one of the four conditions [i.e., one of the four inequalities (4)–(7)] holds

$$\begin{cases} v_i\left(a\sin\psi_i - R_1\frac{\kappa(p_i)\cos\psi_i}{1-\kappa(p_i)\rho_i}\right) + R_1\omega_i + R_1\alpha \le 0 \\ \rho_i \ge 0, \quad \psi_i \ge 0 \end{cases} \tag{4}$$

$$\begin{cases} \omega_i - \frac{\kappa(p_i)v_i\cos\psi_i}{1-\kappa(p_i)\rho_i} + \alpha \le 0 \\ \rho_i < 0, \quad \psi_i > 0 \end{cases} \tag{5}$$

$$\begin{cases} v_i\left(a\sin\psi_i - R_1\frac{\kappa(p_i)\cos\psi_i}{1-\kappa(p_i)\rho_i}\right) + R_1\omega_i - R_1\alpha \ge 0 \\ \rho_i \le 0, \quad \psi_i \le 0 \end{cases} \tag{6}$$

$$\begin{cases} \omega_i - \frac{\kappa(p_i)v_i\cos\psi_i}{1-\kappa(p_i)\rho_i} - \alpha \ge 0 \\ \rho_i > 0, \quad \psi_i < 0 \end{cases} \tag{7}$$

where α is a small positive number.

Lemma 2 can be easily derived by using Lemma 1.

With Lemma 2, we can get an important inequality for the parameter selection, given in the following lemma.

Lemma 3: If there exists $v_m \in (v_{\min}, v_{\max}]$ making (8) and (9) hold, then for any $\phi_i \in \partial\mathcal{S}_1$, there exist v_i and ω_i satisfying (2), such that one of the four inequalities (4)–(7) holds

$$\sqrt{\left(\frac{a}{R_1}\right)^2 + \kappa_0^2} + \frac{\alpha}{v_m} \le \frac{\omega_{\max}}{v_m} \tag{8}$$

$$\frac{\kappa_0}{1 - \kappa_0 R_1} + \frac{\alpha}{v_m} \le \frac{\omega_{\max}}{v_m}. \tag{9}$$

Proof: See Appendix A. ∎

2) Second Principle: We need to guarantee the existence of a proper control law, which ensures the sequence of the UAVs along the path to be fixed, once all the UAVs enter $\mathcal{S}_1$. More specifically, if UAV i and its preneighbor UAV j satisfy $\phi_i(t_0), \phi_j(t_0) \in \mathcal{S}_1$ at time t_0, then there will be no any other kth UAV ($k \ne i, k \ne j$) turning to be the preneighbor of the

ith UAV from then on. Mathematically, if $\phi_i(t_0) \in \mathcal{S}_1 \ \forall \ i = 1, \ldots, n$, then $\zeta_i(t) > 0 \ \forall \ t > t_0$.[1]

Lemma 4: The second principle holds if

$$\frac{1}{1-\kappa_0 R_1} v_{\min} + c \leq \frac{\cos a}{1+\kappa_0 R_1} v_m \tag{10}$$

where $c > 0$.

Proof: See Appendix B. ∎

Besides inequalities (8)–(10) (deduced from Lemmas 3 and 4, respectively), there are some additional constraints for parameters

$$\begin{cases} 0 < a < \pi/2 \\ 0 < R_1 < R_0 \\ v_{\min} < v_m \leq v_{\max}. \end{cases} \tag{11}$$

There are three parameters in (11) left unknown, namely, a, R_1, and v_m. The selection of a, R_1, and v_m can be regarded as an optimization problem. Its objective is to make $\mathcal{S}_1$ as large as possible, since a larger $\mathcal{S}_1$ contains more path-following errors, which means more situations can be directly[2] dealt with our proposed coordination control law in Section III-B. This optimization problem is described by

$$\begin{aligned} &\text{maximize} \quad aR_1 \\ &\text{s.t.} \quad \text{inequalities (8)–(11) hold.} \end{aligned} \tag{12}$$

If constraints (8)–(11) are satisfied (see Lemma 5), we can guarantee the existence of the proper control law satisfying the aforementioned two principles. By solving the optimization problem (12), we can select the optimized parameters a and R_1 to design $\mathcal{S}_1$, and we can also obtain v_m, which is an important parameter in the control law proposed in Section III-B.

Lemma 5: A sufficient condition to guarantee the existence of feasible solutions of (12) is

$$\begin{cases} \kappa_0 \leq \frac{\omega_{\max}}{v_{\max}} \\ v_{\min} + c \leq v_{\max}. \end{cases} \tag{13}$$

Remark 5: Lemma 5 can be verified easily. From it, we can get one guideline to choose the user-determined value of parameter c in (12) as $c \leq v_{\max} - v_{\min}$.

It is obvious from (10) that the smaller c is, the larger the coordination set will become, since we will get a larger feasible region in (12). However, in terms of the control law designs, c is not the smaller the better, because c is also correlated to the convergence rate (more details are given in Section III-B), and a tradeoff should be made between the coordination set's size and the convergence rate.

The above completes the parameter selection process for coordination set $\mathcal{S}_1$. With the parameter selection, we can not only guarantee the existence of the control law satisfying the proposed two principles but also design a proper coordination set $\mathcal{S}_1$. Next, we will design the control law and show the importance of the two principles to the convergence of the path-following error and the sequenced inter-UAV arc distance.

[1]We note that when $\zeta_i(t)$ is reduced to zero, it means the ith UAV is being overtaken by another UAV, or is overtaking another UAV at time t.

[2]We note that if a path-following error is outside $\mathcal{S}_1$, we have to make it enter $\mathcal{S}_1$, before the coordination control law in Section III-B is applied.

Algorithm 1 Coordinated Path-Following Control Law in $\mathcal{S}_1$

Input: $\rho_i, \psi_i, \kappa(p_i), \zeta_i$
Output: v_i, ω_i
1: **procedure** CoordControl($\rho_i, \psi_i, \kappa(p_i), \zeta_i$)
2: Set the forward speed as

$$v_i = \text{Sat}\Big(\frac{1-\kappa(p_i)\rho_i}{\cos\psi_i}\chi(\zeta_i), v_{\min}, v_{\max}\Big);$$

3: Set the angular speed as

$$\omega_i = \text{Sat}(\omega_d, -\omega_{\max}, \omega_{\max}),$$

where

$$\omega_d = v_i\Big[-\frac{k_1\vartheta_i}{k_2} + \frac{\kappa(p_i)\cos\psi_i}{1-\kappa(p_i)\rho_i}\Big] - \alpha\cdot\text{sign}(\vartheta_i),$$

and $k_1 > 0$, $k_2, k_3 \geq 1$ and $a \leq R_1 k_1 < a k_2$;
4: $v_i \leftarrow$ReSetValue($v_i, \omega_i, \rho_i, \psi_i, \kappa(p_i), \zeta_i$)
5: **return** v_i, ω_i
6: **end procedure**
7: **procedure** ReSetValue($v_i, \omega_i, \rho_i, \psi_i, \kappa(p_i), \zeta_i$)
8: **if** $\phi_i \in \mathcal{S}_1^1$ **and** inequality (4) does not hold **then**
9: $v_i = -\Big[a\sin\psi_i - R_1\frac{\kappa(p_i)\cos\psi_i}{1-\kappa(p_i)\rho_i}\Big]^{-1} R_1(\omega_i + \alpha)$
10: **end if**
11: **if** $\phi_i \in \mathcal{S}_1^2$ **and** inequality (5) does not hold **then**
12: $v_i = \frac{1-\kappa(p_i)\rho_i}{\kappa(p_i)\cos\psi_i}(\omega_i + \alpha)$
13: **end if**
14: **if** $\phi_i \in \mathcal{S}_1^3$ **and** inequality (6) does not hold **then**
15: $v_i = -\Big[a\sin\psi_i - R_1\frac{\kappa(p_i)\cos\psi_i}{1-\kappa(p_i)\rho_i}\Big]^{-1} R_1(\omega_i - \alpha)$
16: **end if**
17: **if** $\phi_i \in \mathcal{S}_1^4$ **and** inequality (7) does not hold **then**
18: $v_i = \frac{1-\kappa(p_i)\rho_i}{\kappa(p_i)\cos\psi_i}(\omega_i - \alpha)$
19: **end if**
20: **if** $\phi_i \in \mathcal{S}_1^5$ **and** $\omega_i - \frac{\kappa(p_i)v_i\cos\psi_i}{1-\kappa(p_i)\rho_i} - \alpha < 0$ **then**
21: $v_i = \frac{1-\kappa(p_i)\rho_i}{\kappa(p_i)\cos\psi_i}(\omega_i - \alpha)$
22: **end if**
23: **if** $\phi_i \in \mathcal{S}_1^6$ **and** $\omega_i - \frac{\kappa(p_i)v_i\cos\psi_i}{1-\kappa(p_i)\rho_i} + \alpha > 0$ **then**
24: $v_i = \frac{1-\kappa(p_i)\rho_i}{\kappa(p_i)\cos\psi_i}(\omega_i + \alpha)$
25: **end if**
26: **return** v_i
27: **end procedure**

B. Control Law in $\mathcal{S}_1$

Now, we propose the coordinated path-following control law in $\mathcal{S}_1$, which is included in Algorithm 1. We assume ρ_i, ψ_i, and $\kappa(p_i)$ can be calculated by the UAV itself, since the path is globally available to the UAV. Besides, ζ_i can be measured by the UAV itself or through communication with its preneighbor and, thus, the multi-UAV coordination can be achieved through sensing or communication. When the ith UAV does not have a preneighbor, we artificially set $\zeta_i = L$, i.e., the coordination error $L - \zeta_i$ is set to be zero.

Before illustrating our control algorithm, we introduce a continuous function $\chi(\zeta_i)$, which is used in line 2 with the following properties.

1) $\chi(\zeta_i) = [1/(1-\kappa_0 R_1)]v_{\min}$, when $\zeta_i \in [0, L-\delta_1)$, where $0 < \delta_1 < L$.
2) $\chi(L) = [\lambda/(1-\kappa_0 R_1)]v_{\min} + [((1-\lambda)\cos a)/(1+\kappa_0 R_1)]v_m$, where $0 < \lambda < 1$.
3) $\chi(\zeta_i)$ is nondecreasing when $\zeta_i \in [0, \infty)$, and is strictly increasing in $[L-\delta_2, L+\delta_2]$, where $0 < \delta_2 \leq \delta_1$.

We also use a saturation function $\text{Sat}(\cdot)$ in lines 2 and 3, which is defined as follows (suppose $a < b$): $\text{Sat}(x, a, b) = a$

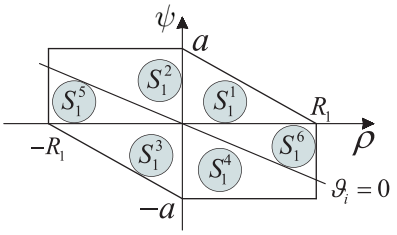

Fig. 3. Six subsets of $\mathcal{S}_1$ divided by $\vartheta_i = 0$, ρ-axis, and ψ-axis.

if $x \le a$, $\mathrm{Sat}(x, a, b) = x$ if $a < x \le b$, and $\mathrm{Sat}(x, a, b) = b$ if $x > b$.

The main procedure of the coordinated path-following algorithm in $\mathcal{S}_1$, CoordControl, can be described as follows: in line 2, we set the value of $v_i \in [v_{\min}, v_{\max}]$ based on the coordination error. We calculate $\omega_i \in [-\omega_{\max}, \omega_{\max}]$ in line 3, which is a function of v_i derived in line 2. After calculating v_i and ω_i, we check whether some properties (see procedure ReSetValue) hold with the derived v_i and ω_i, and if not, we will recalculate v_i again. The checking-recalculating process is depicted by procedure ReSetValue. In this procedure, we divide $\mathcal{S}_1$ into six subsets, and reset the value of v_i by using different rules for different subsets.

Let $\vartheta_i = k_1\rho_i + k_2\psi_i + k_3 \sin\psi_i$, then $\vartheta_i = 0$ is a nearly straight curve passing through the origin, $\vartheta_i > 0$ is on the upper-right side of the curve, and $\vartheta_i < 0$ on its lower-left side. $\vartheta_i = 0$ together with the ρ-axis and the ψ-axis divides $\mathcal{S}_1$ into six subsets as shown in Fig. 3, which are defined as follows:

$$\begin{aligned}
\mathcal{S}_1^1 &= \{\phi_i \in \mathcal{S}_1 : \rho_i > 0, \psi_i \ge 0, \vartheta_i > 0\}\\
\mathcal{S}_1^2 &= \{\phi_i \in \mathcal{S}_1 : \rho_i \le 0, \psi_i \ge 0, \vartheta_i \ge 0\}\\
\mathcal{S}_1^3 &= \{\phi_i \in \mathcal{S}_1 : \rho_i < 0, \psi_i \le 0, \vartheta_i < 0\}\\
\mathcal{S}_1^4 &= \{\phi_i \in \mathcal{S}_1 : \rho_i \ge 0, \psi_i \le 0, \vartheta_i \le 0\}\\
\mathcal{S}_1^5 &= \{\phi_i \in \mathcal{S}_1 : \rho_i < 0, \psi_i > 0, \vartheta_i < 0\}\\
\mathcal{S}_1^6 &= \{\phi_i \in \mathcal{S}_1 : \rho_i > 0, \psi_i < 0, \vartheta_i > 0\}.
\end{aligned}$$

We note that according to the above partition, the origin is contained both in $\mathcal{S}_1^2$ and in $\mathcal{S}_1^4$.

In ReSetValue, we check whether one of the four inequalities (4)–(7) holds when $\phi_i \in \mathcal{S}_1^1 \cup \mathcal{S}_1^2 \cup \mathcal{S}_1^3 \cup \mathcal{S}_1^4$. If not, we will recalculate v_i. It is easy to find that the recalculated v_i can finally make one of the inequalities (4)–(7) hold when $\phi_i \in \mathcal{S}_1^1 \cup \mathcal{S}_1^2 \cup \mathcal{S}_1^3 \cup \mathcal{S}_1^4$. We also note that there is no need to check inequalities (4)–(7) when $\phi_i \in \mathcal{S}_1^5 \cup \mathcal{S}_1^6$, since ϕ_i will not leave $\mathcal{S}_1$ from $|\rho_i| = R_1$ (see Remark 4). But we will make sure $\dot\psi_i \ge 0$ when $\phi_i \in \mathcal{S}_1^5$, and $\dot\psi_i \le 0$ when $\phi_i \in \mathcal{S}_1^6$.

There is an important property of procedure ReSetValue.

Lemma 6: If v_i is changed in ReSetValue, denote v_{i1} as the forward speed calculated in line 2, and v_i is the final returned value from ReSetValue, then $v_m \le v_i < v_{i1}$.

Proof: See Appendix C. ∎

According to the definition of function $\mathrm{Sat}(\cdot)$, we have $v_{i1} \le v_{\max}$. Therefore, Lemma 6 implies that control inputs v_i and ω_i calculated by Algorithm 1 satisfy (2).

We now show that the first principle is guaranteed by using Algorithm 1, which means $\mathcal{S}_1$ is made an invariant set.

Theorem 1 (Validation for the First Principle): According to Algorithm 1, v_i and ω_i make $\mathcal{S}_1$ an invariant set, i.e., if $\phi_i(t_0) \in \mathcal{S}_1$, then $\phi_i(t) \in \mathcal{S}_1 \ \forall\ t > t_0$.

Proof: It is easy to check that procedure ReSetValue can guarantee one of the four inequalities (4)–(7) hold when $\phi_i \in \mathcal{S}_1^1 \cup \mathcal{S}_1^2 \cup \mathcal{S}_1^3 \cup \mathcal{S}_1^4$. According to the definition of these sets, $\partial\mathcal{S}_1 \subsetneq \mathcal{S}_1^1 \cup \mathcal{S}_1^2 \cup \mathcal{S}_1^3 \cup \mathcal{S}_1^4$. With Lemma 2, we can conclude that $\mathcal{S}_1$ is an invariant set. ∎

Remark 6: We get the following results with Algorithm 1.

1) If $\vartheta_i > 0$, then $\dot\psi_i \le -\alpha$; if $\vartheta_i < 0$, then $\dot\psi_i \ge \alpha$.
2) If $\phi_i \in \mathcal{S}_1^1 \cup \mathcal{S}_1^3$, and $\psi_i \ne 0$, then $(\dot\psi_i/\dot\rho_i) \le -(a/R_1)$.

In terms of the second principle proposed in Section III-A, Theorem 2 illustrates that Algorithm 1 guarantees the sequence of UAVs becoming fixed, once all the UAVs enter $\mathcal{S}_1$.

Theorem 2 (Validation for the Second Principle): Suppose $\phi_i(t_0) \in \mathcal{S}_1\ \forall\ i = 1, \ldots, n$. By executing Algorithm 1, if $\zeta_i(t_0) > 0$, then $\zeta_i(t) > 0$ holds $\forall\ t \ge t_0$.

Proof: First, each UAV's speed along the path v_i^r is not smaller than $\chi(0)$ with Algorithm 1. This is obvious if the value of v_i is not changed in ReSetValue by using the definition of $\chi(\cdot)$. If the value of v_i is changed in ReSetValue, according to Lemma 6, $v_i \ge v_m$, then $v_i^r \ge v_m[(\cos a)/(1 + \kappa_0 R_1)] > \chi(0)$.

Now let the jth UAV be the preneighbor of the ith UAV, then $\dot\zeta_i = v_j^r - v_i^r$. Suppose initially $0 < \zeta_i(t_0) \le L - \delta_1$ and, thus, $v_i^r = \chi(0)$. Using similar analyses with Lemma 4, it can be concluded that $\zeta_i(t) > 0\ \forall\ t \ge t_0$. ∎

Now, we show the importance of the two principles to the convergence of the path-following error and sequenced inter-UAV arc distance in $\mathcal{S}_1$. In terms of the path-following error, we have the following theorem stating that all the UAVs will finally move on the desired path if they are all in $\mathcal{S}_1$ initially.

Theorem 3 (Convergence of Path-Following Error): By executing Algorithm 1, if $\phi_i(t_0) \in \mathcal{S}_1$, then $\lim_{t\to\infty} \phi_i(t) = \mathbf{0}$.

Proof: First, recall 1) in Remark 6, $\dot\psi_i \le -\alpha < 0$ when $\vartheta_i > 0$; and $\dot\psi_i \ge \alpha > 0$ when $\vartheta_i < 0$. We note that $\mathcal{S}_1$ is an invariant set according to Theorem 1, and $|\psi_i| \le a$ when $\phi_i \in \mathcal{S}_1$. Therefore, for any $\phi_i(0) \in \mathcal{S}_1$, there exists a finite time $t_0 \le (2a/\alpha)$, such that $\vartheta_i(t_0) = 0$. Second, by 1) in Remark 6, we can show that for any $\phi_i(t_0) \in \{(\rho_i, \psi_i) : \vartheta_i = 0\}$, ϕ_i will not go to $\mathcal{S}_1^5$ or $\mathcal{S}_1^6$ directly, since $\vartheta_i\dot\vartheta_i = \vartheta_i(k_1\dot\rho_i + k_2\dot\psi_i + k_3\dot\psi_i\cos\psi_i) < 0$ when $\phi_i \in \mathcal{S}_1^5 \cup \mathcal{S}_1^6$. Thus, if $\phi_i(t_0) \in \{(\rho_i, \psi_i) : \vartheta_i = 0\}$, the possibilities for the movement of ϕ_i after t_0 can be partitioned into the following three cases.

Case 1: $\phi_i(t) \in \{(\rho_i, \psi_i) : \vartheta_i = 0\}$ holds for any $t \ge t_0$. Since $\vartheta_i = k_1\rho_i + k_2\psi_i + k_3\sin\psi_i$, it can be rewritten as $\vartheta_i = k_1\rho_i + k_2\arcsin(\dot\rho_i/v_i) + k_3(\dot\rho_i/v_i)$. Denote $h(x) = k_2\arcsin(x/v_i) + k_3(x/v_i), x \in [-v_i\sin a, v_i\sin a]$. Obviously, $h(x)$ is an odd function, and its inverse function $h^{-1}(x)$ exists. Thus, if $\vartheta_i(t) \equiv 0$ holds for all $t \ge t_0$, then $\dot\rho_i = -h^{-1}(k_1\rho_i)$. Since $h(x)$ is a Lipschitz function, there exists a positive constant c_1 such that $|h(x)| \le |c_1 x|$. Then, $|\rho_i(t)| \le |\rho_i(t_0)|\exp[-(k_1/c_1)(t - t_0)]$, meaning $\rho_i(t) \to 0$ as $t \to \infty$. Moreover, $\psi_i(t) \to 0$ since $\vartheta_i(t) = k_1\rho_i + k_2\psi_i + k_3\sin\psi_i \equiv 0$ holds for all $t \ge t_0$.

Case 2: $\phi_i(t) \notin \{(\rho_i, \psi_i) : \vartheta_i = 0\}$ for some $t > t_0$, but $\phi_i(t) \in \mathcal{S}_1^2 \cup \mathcal{S}_1^4\ \forall t > t_0$. In this case, since $\dot\psi_i \ge \alpha$ if $\phi_i \in \mathcal{S}_1^4 \setminus \{(\rho_i, \psi_i) : \vartheta_i = 0\}$, and $\dot\psi_i \le -\alpha$ if $\phi_i \in$

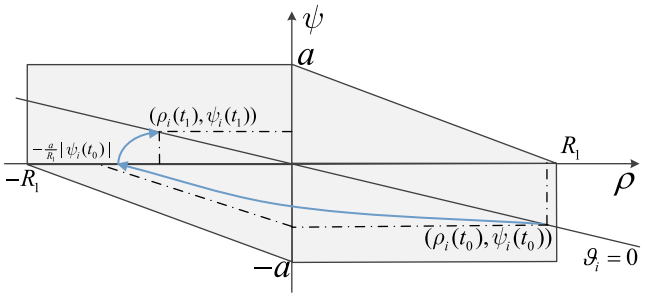

Fig. 4. Illustration of the state trajectory in case 3 when initially $\phi_i(t_0) \in \{(\rho_i, \psi_i) : \vartheta_i = 0\}$.

$\mathcal{S}_1^2 \setminus \{(\rho_i, \psi_i) : \vartheta_i = 0\}$. Therefore, $|\psi_i|$ is nonincreasing when $\phi_i(t) \notin \{(\rho_i, \psi_i) : \vartheta_i = 0\}$, and the total time duration that $\phi_i(t_0) \notin \{(\rho_i, \psi_i) : \vartheta_i = 0\}$ is finite, which is no more than (a/α). Besides, $|\rho_i|$ is also nonincreasing when $\phi_i(t) \notin \{(\rho_i, \psi_i) : \vartheta_i = 0\}$, and by combining the convergence results in case 1, we get $|\rho_i(t)| \leq |\rho_i(t_0)| \exp[-(k_1/c_1)(t - t_0 - (a/\alpha))]$ and, thus, $\lim_{t\to\infty} \rho_i(t) = 0$. Since $|\psi_i|$ is nonincreasing and bounded, then $\lim_{t\to\infty} |\psi_i|$ exists. Note that the total time duration that $\phi_i(t) \notin \{(\rho_i, \psi_i) : \vartheta_i = 0\}$ is finite and $\lim_{t\to\infty} \rho_i(t) = 0$, it leads to $\lim_{t\to\infty} \psi_i(t) = 0$ and, thus, $\lim_{t\to\infty} \phi_i(t) = \mathbf{0}$.

Case 3: there exists $\phi_i(t_0) \in \{(\rho_i, \psi_i) : \vartheta_i = 0\}$ and $\phi_i(t) \notin \mathcal{S}_1^2 \cup \mathcal{S}_1^4$ for some $t > t_0$. Since ϕ_i will not go to $\mathcal{S}_1^5$ and $\mathcal{S}_1^6$ directly, then ϕ_i must have entered $\mathcal{S}_1^1 \cup \mathcal{S}_1^3$ through the ψ-axis. Without loss of generality, we assume $\rho_i(t_0) > 0$ and $\psi_i(t_0) < 0$, as shown in Fig. 4. After ϕ_i enters $\mathcal{S}_1^3$, since $\dot{\psi}_i \geq \alpha > 0$ holds in $\mathcal{S}_1^3$ and $\mathcal{S}_1^5$, there exists a finite time $t_1 \leq t_0 + (2a/\alpha)$ such that $\phi_i(t_1) \in \{(\rho_i, \psi_i) : \vartheta_i = 0\}$, with $\rho_i(t_1) \leq 0$ and $\psi_i(t_1) \geq 0$. We use $(-r_1, 0)$ to denote the intersection of the trajectory of ϕ_i with the ρ-axis, since $\dot{\psi}_i \geq \alpha > 0$ when $\phi_i \in \mathcal{S}_1^4 \setminus \{(\rho_i, \psi_i) : \vartheta_i = 0\}$, and inequality (6) holds when $\phi_i \in \mathcal{S}_1^3$, which means $r_1 < (R_1/a)|\psi_i(t_0)|$. Moreover, since $\dot{\rho}_i = v_i \sin\psi_i > 0$ in $\mathcal{S}_1^5$. Therefore, $|\rho_i(t_1)| < r_1 < (R_1/a)|\psi_i(t_0)|$. We note that $|\psi_i(t_0)| \leq (k_1/k_2)|\rho_i(t_0)|$ and $|\psi_i(t_1)| \leq (k_1/k_2)|\rho_i(t_1)|$. Thus, $|\rho_i(t_1)| < (R_1 k_1/ak_2)|\rho_i(t_0)|$ and $|\psi_i(t_1)| < (R_1 k_1/ak_2)|\psi_i(t_0)|$. Let $\sigma := (R_1 k_1/ak_2)$, and we have $\sigma < 1$. Therefore, $|\rho_i(t)| \leq |\rho_i(t_0)|$, $|\psi_i(t)| \leq |\psi_i(t_0)|$ when $t \in [t_0, t_1]$. By symmetry, when $\phi_i(t_1) \in \{(\rho_i, \psi_i) : \vartheta_i = 0\}$, there are three possibilities for the movement of ϕ_i after t_1, corresponding to the three cases we listed here. We only consider case 3, since the first two cases imply the path-following error converges to zero by our analysis above. Now, if ϕ_i enters $\mathcal{S}_1^1$ after t_1 and then reaches $\{(\rho_i, \psi_i) : \vartheta_i = 0\}$ again at time t_2, it follows that $|\rho_i(t)| \leq \sigma|\rho_i(t_0)|$, $|\psi_i(t)| \leq \sigma|\psi_i(t_0)|$ when $t \in [t_1, t_2]$. Proceeding forward, we get $|\rho_i(t)| \leq \sigma^{m-1}|\rho_i(t_1)|$, and $|\psi_i(t)| \leq \sigma^{m-1}|\psi_i(t_1)|$, for $t \in [t_m, t_{m+1}]$, where t_m corresponds to the mth time that ϕ_i leaves $\mathcal{S}_1^2 \cup \mathcal{S}_1^4$ and reaches $\{(\rho_i, \psi_i) : \vartheta_i = 0\}$ again. Since $\sigma^{m-1} \to 0$ as $m \to \infty$, we get $\lim_{t\to\infty} |\rho_i(t)| = 0$ and $\lim_{t\to\infty} |\psi_i(t)| = 0$, i.e., $\lim_{t\to\infty} \phi_i(t) = \mathbf{0}$.

Combining the above cases together, we conclude that $\lim_{t\to\infty} \phi_i(t) = \mathbf{0}$ always holds. ■

Remark 7: According to the proof of Theorem 3, if $\phi_i(t_0) \in \{(\rho_i, \psi_i) : \vartheta_i = 0\}$, there are three possibilities for the movement of ϕ_i after t_0. However, in a small neighborhood of the origin, it satisfies $k_1 v_{\max}|\sin\psi_i| \leq k_2\alpha + k_3\alpha\cos\psi_i$. As a result, $\vartheta_i\dot{\vartheta}_i \leq 0$ always holds in this neighborhood, and $\vartheta_i\dot{\vartheta}_i = 0$ if and only if $\vartheta_i = 0$, meaning ϕ_i can only slide on $\vartheta_i = 0$ once it reaches $\{(\rho_i, \psi_i) : \vartheta_i = 0\}$ in this neighborhood. We also note that since the signum function is adopted in the control law, ω_i is not continuous at $\vartheta_i = 0$, but ϕ_i is continuous. Thus, the solution should be understood in the sense of Filippov. To eliminate chattering caused by the signum function, a high-slope saturation function can be used to replace it [37].

Remark 8: It should be noted that the Lyapunov method can be employed in each subset of $\mathcal{S}_1$ by considering the following Lyapunov function candidate:

$$V = \begin{cases} \frac{1}{2}(k_1\rho_i + k_2\psi_i + k_3\sin\psi_i)^2, & \phi_i \in \mathcal{S}_1^1 \cup \mathcal{S}_1^3 \\ \frac{1}{2}(k_2\psi_i + k_3\sin\psi_i)^2, & \phi_i \in \mathcal{S}_1^2 \cup \mathcal{S}_1^4 \\ \frac{1}{2}(k_1\rho_i)^2, & \phi_i \in \mathcal{S}_1^5 \cup \mathcal{S}_1^6. \end{cases}$$

It can be found that V is a continuous function of ϕ_i, and $\dot{V} < 0$ in the interior of each subset. However, V is not differentiable with respect to ϕ_i on the boundary of these subsets. Thus, it calls for the similar technique to the above proof to analyze the boundaries in order to conclude the asymptotic stability.

Now, we have demonstrated the path-following stability in $\mathcal{S}_1$. In terms of the coordination, we have the following claim that the coordination error will also converge to zero.

Theorem 4 (Convergence of Coordination Error): Suppose $\phi_i(t_0) \in \mathcal{S}_1 \ \forall\ i = 1, \ldots, n$, by executing Algorithm 1, $\lim_{t\to\infty} \zeta_i(t) = L$ for all i.

Proof: It follows from Theorem 2 that the preneighbor of each UAV does not change. Without loss of generality, suppose UAV 1 is the preneighbor of UAV 2, UAV 2 is the preneighbor of UAV 3, and so on. Since UAV 1 does not have a preneighbor, it is artificially set as $\zeta_1 = L$. For UAV 2, consider $V_2 = (1/2)(\zeta_2 - L)^2$, thus $\dot{V}_2 = (\zeta_2 - L)\dot{\zeta}_2 = (\zeta_2 - L)(v_1^r - v_2^r) = -(\zeta_2 - L)(v_2^r - \chi(L))$. According to the definition of $\chi(\cdot)$ and Lemma 6, $(v_i^r - \chi(L)) \cdot (\zeta_i - L) \geq 0$, and the equality holds if and only if $\zeta_i = L$. Thus, we obtain $\lim_{t\to\infty} \zeta_2(t) = L$ by using LaSalle's invariance principle [37]. As a result, $\lim_{t\to\infty} v_2^r = \chi(L)$. Since $\dot{\zeta}_3 = (v_2^r - \chi(L)) - (v_3^r - \chi(L))$, and the system described by equation $\dot{\zeta}_i = -(v_i^r - \chi(L))$ will converge to $\lim_{t\to\infty} \zeta_i = L$ (we get this claim by using the same analyses for UAV 2), with the limiting equation theorem [38], we get $\lim_{t\to\infty} \zeta_3 = L$. Proceeding forward, we get $\lim_{t\to\infty} \zeta_1(t) = \cdots = \lim_{t\to\infty} \zeta_n(t) = L$. ■

Now, we have completed the control law design in $\mathcal{S}_1$. The designed control law can drive the UAVs whose path-following errors initially in $\mathcal{S}_1$ to move onto the predefined path, with the inter-UAV arc distances converging to the desired value. Recall that in Remark 5, we propose a guideline for the user-determined value c, i.e., the smaller c is, the larger the coordination set would become, since we will get a larger feasible region for (12). However, the value of c is not the smaller, the better. From the perspective of the convergence rate of the coordination error, assume the jth UAV is the preneighbor of the ith UAV, and the coordination error of the jth UAV is

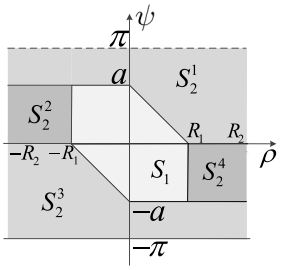

Fig. 5. $\mathcal{S}_1$ and partition of $\mathcal{S}_2$.

already zero, i.e., $\zeta_j = L$. If $\zeta_i < L$, then

$$\left|\dot{\zeta}_i\right| = \left|v_i^r - v_j^r\right| = \left|\chi(\zeta_i) - \chi\left(\zeta_j\right)\right| \leq (1-\lambda)\left[\frac{\cos a}{1+\kappa_0 R_1} v_m - \frac{1}{1-\kappa_0 R_1} v_{\min}\right]. \quad (14)$$

Recall that (10) is a precondition for (12), then with a greater c, we are more likely to have a greater value of $[(\cos a)/(1+\kappa_0 R_1)]v_m - [1/(1-\kappa_0 R_1)]v_{\min}$ from (12), then we can get a greater upper bound for the convergence rate of the coordination error in this case. Therefore, the determination of value c is a tradeoff between enlarging the coordination set and increasing the convergence rate of the sequenced inter-UAV arc distance.

IV. Single-Agent-Level Control Law Outside Coordination Set

In Section III, we have designed the control law for UAVs whose path-following errors are within $\mathcal{S}_1$, such that they follow the path in a coordination manner. For the UAVs whose path-following errors are outside $\mathcal{S}_1$, they have comparatively larger path-following errors. Thus, it is a natural idea to reduce these UAVs' path-following errors first to let them enter $\mathcal{S}_1$, i.e., those UAVs do not follow the path cooperatively, but only adjust their path-following errors at the single-agent level.

We define a universe $\mathcal{S}$ which gives the scope for our designed control law[3]

$$\mathcal{S} = \{(\rho, \psi) : \rho \in [-R_2, R_2], \psi \in [-\pi, \pi)\}. \quad (15)$$

Then, set $\mathcal{S}_2$ is defined as $\mathcal{S}_2 := \mathcal{S} \setminus \mathcal{S}_1$. We further divide $\mathcal{S}_2$ into four subsets: $\mathcal{S}_2^1$, $\mathcal{S}_2^2$, $\mathcal{S}_2^3$, and $\mathcal{S}_2^4$, as shown in Fig. 5. The mathematical descriptions of these subsets are as follows:

$$\begin{aligned}
\mathcal{S}_2^1 &= \left(\{(\rho, \psi) : \psi > 0\} \cap \mathcal{S}_2 \setminus \mathcal{S}_2^2\right) \bigcup \{(\rho, \psi) : R_1 < \rho \leq R_2, \psi = 0\} \\
\mathcal{S}_2^2 &= \{(\rho, \psi) : -R_2 \leq \rho < -R_1, 0 < \psi \leq a\} \\
\mathcal{S}_2^3 &= \left(\{(\rho, \psi) : \psi < 0\} \cap \mathcal{S}_2 \setminus \mathcal{S}_2^4\right) \bigcup \{(\rho, \psi) : -R_2 \leq \rho < -R_1, \psi = 0\} \\
\mathcal{S}_2^4 &= \{(\rho, \psi) : R_1 < \rho \leq R_2, -a \leq \psi < 0\}.
\end{aligned}$$

[3]For the path-following errors outside $\mathcal{S}$, they are distant away from the path Γ, and we can design Dubins paths to drive the errors into $\mathcal{S}$.

In the rest of this section, we design the control laws for these four subsets. In Section IV-A, we prove the existence of the control law which makes any path-following error in sets $\mathcal{S}_2^2$ and $\mathcal{S}_2^4$ enter $\mathcal{S}_1$, and a near time-optimal control law for sets $\mathcal{S}_2^2$ and $\mathcal{S}_2^4$ is designed. In Section IV-B, we design an attraction region-based control law for sets $\mathcal{S}_2^1$ and $\mathcal{S}_2^3$.

A. Near Time-Optimal Control Law in $\mathcal{S}_2^2$ and $\mathcal{S}_2^4$

First, we prove the existence of control laws which makes the path-following error within $\mathcal{S}_2^2 \cup \mathcal{S}_2^4$ enter $\mathcal{S}_1$.

Theorem 5 (Dynamics in $\mathcal{S}_2^2$ and $\mathcal{S}_2^4$): If $R_2 < (1/\kappa_0) - (v_{\min}/\omega_{\max})$, then for any $\phi_i(t_0) \in \mathcal{S}_2^2 \cup \mathcal{S}_2^4$, there exists time t_1, and control $(v_i(t), \omega_i(t))$, $t \in [t_0, t_1]$, satisfying constraint (2), such that $\phi_i(t_1) \in \mathcal{S}_1$.

Proof: Without loss of generality, we consider the condition in $\mathcal{S}_2^4$. The condition in $\mathcal{S}_2^2$ can be deduced similarly.

In $\mathcal{S}_2^4$, since $\psi_i < 0$, then $\dot{\rho}_i < 0$. According to Lemma 1 $\forall\ \phi_i(t_0) \in \mathcal{S}_2^4$ would not leave $\mathcal{S}$ through $\rho = R_2$, thus, it can only enter $\mathcal{S}_1$ through $\rho = R_1$, or enter $\mathcal{S}_2^3$ through $\psi = -a$, or enter $\mathcal{S}_2^1$ through $\psi = 0$, or remain in $\mathcal{S}_2^4$ forever. We show that by applying the appropriate control law, the last three cases can be made impossible. Otherwise, suppose ϕ_i will enter $\mathcal{S}_2^3$, then there exists $\phi_i = (\rho_i, \psi_i)$ such that

$$\dot{\psi}_i = \omega_i - \frac{\kappa(p_i) v_i \cos\psi_i}{1 - \kappa(p_i)\rho_i} < 0 \quad (16)$$

holds for all v_i and ω_i satisfying (2). Let $\omega_i = \omega_{\max}$, $v_i = v_{\min}$, and (16) becomes

$$\omega_{\max} - \frac{\kappa(p_i) v_{\min} \cos\psi_i}{1 - \kappa(p_i)\rho_i} < 0. \quad (17)$$

If $\phi_i \in \mathcal{S}_2^4$, then $\cos\psi_i > 0$ and $1 + \kappa(p_i)\rho_i > 0$ hold, then

$$\begin{aligned}
\omega_{\max} - \frac{\kappa(p_i) v_{\min} \cos\psi_i}{1 - \kappa(p_i)\rho_i} &\geq \omega_{\max} - \frac{\kappa_0 v_{\min} \cos\psi_i}{1 - \kappa_0 \rho_i} \\
&\geq \omega_{\max} - \frac{\kappa_0 v_{\min}}{1 - \kappa_0 R_2} \geq 0 \quad (18)
\end{aligned}$$

which is contrary to (17), meaning there exist v_i and ω_i satisfying (2), such that ϕ_i will not enter $\mathcal{S}_2^3$. In the same way, we conclude that there exist v_i and ω_i such that ϕ_i will not enter $\mathcal{S}_2^1$ if $(\rho_i(t_0), \psi_i(t_0)) \in \mathcal{S}_2^4$, and additionally, it can be made that $\psi_i(t) \leq \psi_i(t_0)$ for all $t \geq t_0$ before ϕ_i leaves $\mathcal{S}_2^4$. Thus, there exists $t_1 \leq [(R_1 - \rho_i(t_0))/(v_{\min} \sin\psi_i(t_0))]$ such that $\phi_i(t_1) \in \mathcal{S}_1$. ∎

Since all the state errors in $\mathcal{S}_2^2$ and $\mathcal{S}_2^4$ can enter $\mathcal{S}_1$ when $R_2 < (1/\kappa_0) - (v_{\min}/\omega_{\max})$, it is necessary to make ϕ_i enter $\mathcal{S}_1$ as soon as possible. Suppose t_f is the minimum time instant such that $\phi_i(t_f) \in \mathcal{S}_1$, then the time optimal control objective is to minimize t_f, which can be formulated as follows:

$$\text{(P1) minimize } J_1 = t_f \quad \text{s.t. } \phi_i(t_0) \in \mathcal{S}_2^2 \cup \mathcal{S}_2^4,\ \phi_i\left(t_f\right) \in \mathcal{S}_1, \text{ and (2) holds.}$$

In general, it is difficult to derive the optimal solution to P1. Here, we adopt a greedy strategy to transform P1 into a near-optimal control problem. Let $d = \inf_{\phi_f \in \mathcal{S}_1} \|\phi_i(t) - \phi_f\|$ denote the point-to-set Euclidean distance from $\phi_i(t)$ to $\mathcal{S}_1$. In our greedy strategy, the control objective is to minimize $\dot{d}$

at every time instant,[4] i.e., to drive $\phi_i(t)$ as close as possible toward $\mathcal{S}_1$. Thus, P1 is transformed to the following problem:

$$\text{(P2) minimize } J_2 = \dot{d}, \text{ where } d = \inf_{\phi_f \in \mathcal{S}_1} \left\| \phi_i(t) - \phi_f \right\|$$
$$\text{s.t. } \phi_i(t) \in \mathcal{S}_2^2 \cup \mathcal{S}_2^4, \text{ and inequality (2) holds.}$$

When $\phi_i(t) \in \mathcal{S}_2^4$, $d = \rho_i - R_1$, then

$$J_2 = \dot{\rho}_i = v_i \sin\psi_i.$$

In $\mathcal{S}_2^4$, $\psi_i < 0$, so $v_i = v_{\max}$. In terms of ω_i, we have

$$\frac{\partial J_2}{\partial \omega_i} = \frac{\partial J_2}{\partial \psi_i} \cdot \frac{\partial \psi_i}{\partial \omega_i} = \frac{\partial J_2}{\partial \psi_i} \cdot \frac{\partial \dot{\psi}_i}{\partial \omega_i} \cdot dt = v_i \cos\psi_i \cdot dt > 0. \tag{19}$$

Therefore, to minimize J_2, we choose $\omega_i = -\omega_{\max}$, and the control law in $\mathcal{S}_2^4$ becomes

$$v_i = v_{\max}, \quad \omega_i = -\omega_{\max}. \tag{20}$$

With the control law (20), we have

$$\dot{\psi}_i = \omega_i - \frac{\kappa(p_i) v_i \cos\psi_i}{1 - \kappa(p_i)\rho_i} = -\omega_{\max} - \frac{\kappa(p_i) v_{\min} \cos\psi_i}{1 - \kappa(p_i)\rho_i}$$
$$\leq -\omega_{\max} + \frac{\kappa_0 v_{\min}}{1 + \kappa_0 R_1} \leq 0. \tag{21}$$

According to Lemma 1, by applying this control law, ϕ_i will not enter $\mathcal{S}_2^1$ through the ρ-axis. However, it may lead ϕ_i to enter $\mathcal{S}_2^3$. To prevent it, we set up a threshold ϵ_0, where $0 < \epsilon_0 \ll a$. When $-a \leq \psi_i < -a + \epsilon_0$, we switch to a new control mode. There are two principles for this new mode. First, we need $\dot{\psi}_i \geq 0$ such that ϕ_i will not enter $\mathcal{S}_2^3$. Second, we need to minimize $\dot{d}$, i.e., $v_i \sin\psi_i$. Thus, the optimization problem P2 becomes (22) when $-a \leq \psi_i < -a + \epsilon_0$

$$\text{minimize } v_i \sin\psi_i$$
$$\text{s.t. } \omega_i - \frac{\kappa(p_i) v_i \cos\psi_i}{1 - \kappa(p_i)\rho_i} \geq 0, \text{ and (2) holds.} \tag{22}$$

Then, our near time-optimal control law in $\mathcal{S}_2^4$ can be described as follows:

1) If $\psi_i \geq -a + \epsilon_0$, the control law is (20).
2) If $-a \leq \psi_i < -a + \epsilon_0$, the control law is the solution of (22), i.e.,
   a) if $\omega_{\max} - [(\kappa(p_i) v_{\max} \cos\psi_i)/(1 - \kappa(p_i)\rho_i)] \geq 0$, then
   $$v_i = v_{\max}, \ \omega_i = \max\left\{-\omega_{\max}, \frac{\kappa(p_i) v_{\max} \cos\psi_i}{1 - \kappa(p_i)\rho_i}\right\}$$
   b) if $\omega_{\max} - [(\kappa(p_i) v_{\max} \cos\psi_i)/(1 - \kappa(p_i)\rho_i)] < 0$, then
   $$v_i = \frac{\omega_{\max}(1 - \kappa(p_i)\rho_i)}{\kappa(p_i)\cos\psi_i}, \quad \omega_i = \omega_{\max}.$$

The control law in $\mathcal{S}_2^2$ can be designed in the same way.

1) If $\psi_i \leq a - \epsilon_0$, the control law is (23)
$$v_i = v_{\max}, \quad \omega_i = \omega_{\max}. \tag{23}$$
2) If $a - \epsilon_0 < \psi_i \leq a$, the control law is the solution of (24)
$$\text{maximize } v_i \sin\psi_i$$
$$\text{s.t. } \omega_i - \frac{\kappa(p_i) v_i \cos\psi_i}{1 - \kappa(p_i)\rho_i} \leq 0, \text{ and (2) holds.} \tag{24}$$

It is easy to verify that the proposed near time-optimal control law is the desired control in Theorem 5, i.e., ϕ_i will enter $\mathcal{S}_1$ when initially in $\mathcal{S}_2^2 \cup \mathcal{S}_2^4$ by executing the control law.

B. Attraction Region-Based Control Law in $\mathcal{S}_2^1$ and $\mathcal{S}_2^3$

By the symmetric property, we only analyze the control law design in $\mathcal{S}_2^1$, and the methods can be applied to $\mathcal{S}_2^3$.

It is obvious by Lemma 1 that $\mathcal{S}_2^1$ is not an invariant set. Specifically, there are five situations that $\phi_i(t)$ leaves $\mathcal{S}_2^1$.

1) $\phi_i(t)$ passes through $\psi = a, -R_1 \leq \rho < 0$, or $a\rho + R_1\psi = aR_1, 0 \leq \rho \leq R_1$, and enters $\mathcal{S}_1$ directly.
2) $\phi_i(t)$ passes through $\psi = a, -R_2 \leq \rho < -R_1$, and enters $\mathcal{S}_2^2$.
3) $\phi_i(t)$ passes through $\psi = 0, R_1 < \rho \leq R_2$, and enters $\mathcal{S}_2^4$.
4) $\phi_i(t)$ passes through $\psi = \pi$, and enters $\mathcal{S}_2^3$.
v) $\phi_i(t)$ passes through $\rho = R_2, 0 \leq \psi \leq \pi$, and leaves $\mathcal{S}$.

Among all these situations, situation 1) is the case that $\phi_i(t)$ enters $\mathcal{S}_1$ directly. For situations 2) and 3), $\phi_i(t)$ enters $\mathcal{S}_2^2$ or $\mathcal{S}_2^4$, which can finally enter $\mathcal{S}_1$ (see Theorem 5). For situation 5), $\phi_i(t)$ leaves $\mathcal{S}$. For situation 4), $\phi_i(t)$ enters $\mathcal{S}_2^3$, which has the same property as that in $\mathcal{S}_2^1$ due to the symmetric property. We note that for situation 4), it still has the possibility to make $\phi_i(t)$ leave $\mathcal{S}$. Hence, we propose an attraction region-based control law to avoid the last two situations. More specifically, our objective is to maximize the possibility of the trajectory belonging to the first three situations.

Denote the ratio of $\dot{\psi}_i$ and $\dot{\rho}_i$ as β_i, i.e., $\beta_i = (\dot{\psi}_i/\dot{\rho}_i)$. We note that a smaller β_i can make $\phi_i \in \mathcal{S}_2^1$ have a higher possibility of belonging to the first three situations. This is because β_i determines the tangent to the state trajectory, and a smaller β_i corresponds to a steeper slope toward the ρ-axis, which maximizes the possibility of the trajectory entering $\mathcal{S}_1 \cup \mathcal{S}_2^2 \cup \mathcal{S}_4^2$. In this way, the control problem in $\mathcal{S}_2^1$ is formulated as

$$\text{minimize } \frac{\omega_i}{v_i \sin\psi_i} - \frac{\kappa(p_i)\cot\psi_i}{1 - \kappa(p_i)}$$
$$\text{s.t. } \phi_i(t) \in \mathcal{S}_2^1, \text{ and (2) holds}$$

and the solution is

$$v_i = v_{\min}, \quad \omega_i = -\omega_{\max}. \tag{25}$$

Similarly, the control law in $\mathcal{S}_2^3$ can be derived as

$$v_i = v_{\min}, \quad \omega_i = \omega_{\max}. \tag{26}$$

Then, we provide a sufficient condition for states in $\mathcal{S}_2^1$ entering $\mathcal{S}_1$ finally.

Theorem 6 (Dynamics in $\mathcal{S}_2^1$): Consider the system described by state equations (27) and (28), where the state variables are denoted as $\tilde{\phi}_i = (\tilde{\rho}_i, \tilde{\psi}_i)$. If $\tilde{\phi}_i(t_0) = \phi_i(t_0) \in \mathcal{S}_2^1$, and the state trajectory of $\tilde{\phi}_i$ has an intersection with the $\tilde{\rho}$-axis,

[4]This is why we say this strategy is "greedy."

denoted as $(R^*, 0)$, where $R^* \leq R_2 < (1/\kappa_0) - (v_{\min}/\omega_{\max})$, then for any $\phi_i(t_0) \in \mathcal{S}_2^1$, by applying the control law (25), ϕ_i will get into $\mathcal{S}_1 \cup \mathcal{S}_2^2 \cup \mathcal{S}_2^4$ in a finite time

$$\begin{cases} \dot{\tilde{\rho}}_i = v_{\min} \sin \tilde{\psi}_i \\ \dot{\tilde{\psi}}_i = -\omega_{\max} - \frac{\kappa_0 v_{\min} \cos \tilde{\psi}_i}{1-\kappa_0 \tilde{\rho}_i}, \end{cases} \quad \pi/2 \leq \tilde{\psi}_i < \pi \tag{27}$$

$$\begin{cases} \dot{\tilde{\rho}}_i = v_{\min} \sin \tilde{\psi}_i \\ \dot{\tilde{\psi}}_i = -\omega_{\max} + \frac{\kappa_0 v_{\min} \cos \tilde{\psi}_i}{1+\kappa_0 \tilde{\rho}_i}, \end{cases} \quad 0 \leq \tilde{\psi}_i < \pi/2. \tag{28}$$

Proof: The state trajectory of $\tilde{\phi}_i$ after t_0 can be described by $g(\phi_i) = 0$, with the gradient vector $\nabla g(\phi_i) = (-\dot{\tilde{\psi}}_i, \dot{\tilde{\rho}}_i)$. Since $g(\phi_i) = 0$ has an intersection with the $\tilde{\rho}$-axis at $(R^*, 0)$, where $R^* \leq R_2$, then $g(\phi_i) = 0$ lies in $\mathcal{S}$ when $\tilde{\psi}_i \in [0, \pi)$. By applying the control law (25), $\dot{\rho}_i = v_{\min} \sin \psi_i$, $\dot{\psi}_i = -\omega_{\max} - [(\kappa(p_i) v_{\min} \cos \psi_i)/(1 - \kappa(p_i)\rho_i)]$. Suppose $g(\phi_i(t)) = 0$ at time t, where $t \geq t_0$, and $\phi_i(t) \in \mathcal{S}_2^1$, it can be verified that $f(\phi_i) \cdot \nabla g(\phi_i) \leq 0$ holds. With Lemma 1, we conclude that the state trajectory of ϕ_i is bounded by $g(\phi_i) = 0$ when $\phi_i \in \mathcal{S}_2^1$, i.e., ϕ_i will not leave $\mathcal{S}$. Let $\alpha_1 = \omega_{\max} - [(\kappa_0 v_{\min})/(1 - \kappa_0 R_2)]$, and we have $\alpha_1 > 0$. By applying control law (25), $\dot{\tilde{\psi}}_i \leq -\alpha_1 < 0$ when $\phi_i \in \mathcal{S}_2^1$. Thus, there exists a finite time $t_1 \leq t_0 + (\pi/\alpha_1)$, such that $\phi_i(t_1) \in \mathcal{S}_1 \cup \mathcal{S}_2^2 \cup \mathcal{S}_2^4$. ∎

For states in $\mathcal{S}_2^3$, we have a similar result.

Theorem 7 (Dynamics in $\mathcal{S}_2^3$): Consider the system described by state equations (29) and (30), where the state variables are denoted as $\tilde{\phi}_i = (\tilde{\rho}_i, \tilde{\psi}_i)$. If $\tilde{\phi}_i(t_0) = \phi_i(t_0) \in \mathcal{S}_2^3$, and the state trajectory of $\tilde{\phi}_i$ has an intersection with the $\tilde{\rho}$-axis, denoted as $(-R^*, 0)$, where $R^* \leq R_2 < (1/\kappa_0) - (v_{\min}/\omega_{\max})$. then for any $\phi_i(t_0) \in \mathcal{S}_2^3$, by applying control law (26), ϕ_i will get into $\mathcal{S}_1 \cup \mathcal{S}_2^2 \cup \mathcal{S}_2^4$ in a finite time

$$\begin{cases} \dot{\tilde{\rho}}_i = v_{\min} \sin \tilde{\psi}_i \\ \dot{\psi}_i = \omega_{\max} + \frac{\kappa_0 v_{\min} \cos \tilde{\psi}_i}{1+\kappa_0 \tilde{\rho}_i}, \end{cases} \quad -\pi \leq \tilde{\psi}_i < -\pi/2 \tag{29}$$

$$\begin{cases} \dot{\tilde{\rho}}_i = v_{\min} \sin \tilde{\psi}_i \\ \dot{\psi}_i = \omega_{\max} - \frac{\kappa_0 v_{\min} \cos \tilde{\psi}_i}{1-\kappa_0 \tilde{\rho}_i}, \end{cases} \quad -\pi/2 \leq \tilde{\psi}_i \leq 0. \tag{30}$$

After ϕ_i enters $\mathcal{S}_2^2 \cup \mathcal{S}_2^4$, it is certain that following our proposed control law in these two subsets (see Section IV-A), ϕ_i can finally enter $\mathcal{S}_1$. We have the following theorem to conclude the stability and convergence of the overall closed-loop system.

Theorem 8: Consider a fleet of fixed-wing UAVs following a $\mathcal{C}^2$-smooth path under Assumption 1, with the path-following error equation described by (3) with constraints (2). If $R_2 < (1/\kappa_0) - (v_{\min}/\omega_{\max})$, and each UAV is in one of the following cases.

1) *Case 1:* $\phi_i(t_0) \in \mathcal{S}_1$.
2) *Case 2:* $\phi_i(t_0) \in \mathcal{S}_2^2 \cup \mathcal{S}_2^4$.
3) *Case 3:* $\phi_i(t_0) \in \mathcal{S}_2^1$, and the state trajectory of $\tilde{\phi}_i$ following (27) and (28) has an intersection with the $\tilde{\rho}$-axis at $(R^*, 0)$, where $R^* \leq R_2$, when $\tilde{\phi}_i(t_0) = \phi_i(t_0)$.
4) *Case 4:* $\phi_i(t_0) \in \mathcal{S}_2^3$, and the state trajectory of $\tilde{\phi}_i$ following (29) and (30) has an intersection with the $\tilde{\rho}$-axis at $(-R^*, 0)$, where $R^* \leq R_2$, when $\tilde{\phi}_i(t_0) = \phi_i(t_0)$

then by executing Algorithm 1 when $\phi_i(t) \in \mathcal{S}_1$, control law (20) and (22) when $\phi_i(t) \in \mathcal{S}_2^4$, control law (23) and (24) when $\phi_i(t) \in \mathcal{S}_2^2$, control law (25) when $\phi_i(t) \in \mathcal{S}_2^1$, and control law (26) when $\phi_i(t) \in \mathcal{S}_2^3$, we will finally get $\lim_{t\to\infty} \phi_i = \mathbf{0}$, $\lim_{t\to\infty} \zeta_i = L \ \forall \ i$.

Note that the proposed controller in Theorem 8 for the overall system is hybrid, as the controller is not continuous at the boundary of the subsets. For example, when ϕ_i enters $\mathcal{S}_1$ from $\mathcal{S}_4^2$ at time t_a, and $\psi_i(t_a) \geq -a + \epsilon_0$, then according to (20), $\lim_{t\to t_a^-} v_i = v_{\max}$, and $\lim_{t\to t_a^-} \omega_i = -\omega_{\max}$. However, it does not necessarily return $v_i = v_{\max}$ and $\omega_i = \omega_{\max}$ with Algorithm 1 at time t_a. Now, it is the position to analyze the stability of Theorem 8.

Proof: The convergence of the closed-loop system can be concluded by using a similar technique with [2, Th. 3.5]. In each of the last three cases, ϕ_i will enter the coordination set, i.e., satisfies the condition in case 1, within a finite time.

1) For case 2, by Theorem 5, there exists a time $t_1 \geq t_0$ such that $\phi_i(t_1) \in \mathcal{S}_1$.
2) For cases 3 and 4, by Theorems 6 and 7, there exists a time $t_2 \geq t_0$ such that $\phi_i(t_2) \in \mathcal{S}_1 \cup \mathcal{S}_2^2 \cup \mathcal{S}_4^2$; if $\phi_i(t_2) \in \mathcal{S}_2^2 \cup \mathcal{S}_4^2$, by Theorem 5, there exists a time $t_3 \geq t_2 \geq t_0$ such that $\phi_i(t_3) \in \mathcal{S}_1$.

While for case 1, by Theorem 1, ϕ_i remains in $\mathcal{S}_1$ thereafter. Consequently, there exists a time $t^* \geq t_0$ such that $\phi_i(t^*) \in \mathcal{S}_1$ holds for all i. Thus, following Theorem 3, we get $\lim_{t\to\infty} \phi_i = \mathbf{0}$, and following Theorem 4, we get $\lim_{t\to\infty} \zeta_i = L$. ∎

Remark 9: We note that collisions between UAVs can be avoided if the path has no intersection points and the UAVs are inside the coordination set, since no overtaking will occur according to Theorem 2. However, when the UAVs are outside the coordination set, since they are executing the single-agent level control law, collision avoidance is not guaranteed. In real applications, we can set up a collision-avoidance-related threshold. When the distance from a UAV to another UAV is less than this threshold, the UAV can execute the collision-avoidance algorithm such as the method in [39], and the UAV's forward speed can be set as the value when it switches to the collision-avoidance mode. When the distance to another UAV is greater than this threshold, the UAV executes the single-agent level control law proposed in this section.

V. Simulation Results

In this section, simulations are given to corroborate the effectiveness of our control strategy for a coordinated path following. The simulation consists of two parts: 1) numerical simulation and 2) the HIL simulation with the X-Plane simulator.

A. Numerical Simulation

First, we validate the algorithm with a typical path-following problem, the cyclic pursuit on a circle. The control objective is to distribute all the UAVs uniformly on a circle. The UAVs are with the constraints $v_{\min} = 10$ m/s, $v_{\max} = 25$ m/s, and $\omega_{\max} = 0.2$ rad/s. The desired path is a circle centered at $(0, 0)$, with the radius of $r = 1000$ m. We are employing $n = 6$ UAVs in the simulation, then the desired arc distance is $L = 2\pi r/n = 1000\pi/3$ m. We take $\kappa_0 = 0.002$, then the optimized parameters for the coordination set are

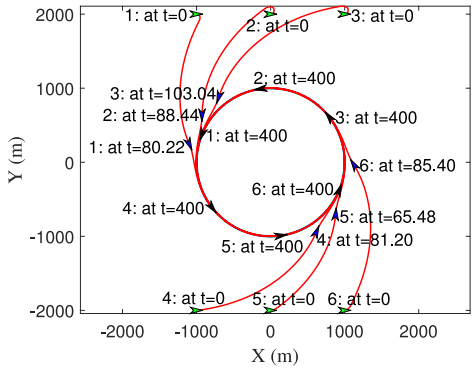

Fig. 6. Trajectories of six UAVs following a circle, with the green wedges indicating the initial positions and headings for each UAV, blue ones indicating the states when each UAV enters $\mathcal{S}_1$, and black ones indicating the final states.

$a = 0.6303$ and $R_1 = 122.1297$. We take control parameters $c = 3$, $k_1 = 1$, $k_2 = R_1/a + 1$, $k_3 = 1$, and $\epsilon_0 = 0.05$. The initial positions of the six UAVs are $(-1000, 2000)^T$, $(0, 2000)^T$, $(1000, 2000)^T$, $(-1000, -2000)^T$, $(0, -2000)^T$, $(1000, -2000)^T$, and $\theta_i = 0$, $i = 1, \ldots, 6$. $\chi(\zeta_i)$ is defined as

$$\chi(\zeta_i) = \begin{cases} v^r_{\min}, & \text{when } \zeta_i < L - 6 \\ 0.475(\zeta_i - L + 6) + v^r_{\min}, & \text{when } |\zeta_i - L| \le 6 \\ 0.95(\zeta_i - L) + v^r_{\min}, & \text{otherwise} \end{cases}$$

where $v^r_{\min} = [1/(1 - \kappa_0 R_1)]v_{\min}$.

The trajectories of the six UAVs under our hybrid control law are shown in Fig. 6. The wedges in the figure not only indicate the positions of the UAVs but also their headings. The green wedges represent the initial positions and headings for the UAVs. Initially, $\phi_1(0) \in \mathcal{S}^1_2$, $\phi_4(0) \in \mathcal{S}^2_2$, and $\phi_2(0), \phi_3(0), \phi_5(0), \phi_6(0) \in \mathcal{S}^3_2$. By executing the single-agent level control law designed in Section IV, ϕ_i, $i = 1, \ldots, 6$ all enter the coordination set $\mathcal{S}_1$. The blue wedges in Fig. 6 represent the positions and headings at the time when each UAV enters $\mathcal{S}_1$, and the UAVs at $t = 400$ s are shown by the black wedges. We can see that all the UAVs are finally distributed uniformly on the circular path by executing the coordinated control law designed in Section III.

Fig. 7 shows the coordinated path-following performance of each UAV, where all the UAVs' ρ_i and ψ_i converge to zero, and ζ_i converges to the expected value. Fig. 8 shows the control inputs of each UAV. It can be observed that the control input constraints are satisfied.

To evaluate the real-time performance of the proposed algorithm, the simulation is conducted 1000 times using the MATLAB software on a laptop with 2.6-GHz Intel dual-core CPU and 8-GB RAM. The MATLAB version is R2016a. In each simulation, there are 40 000 steps for each UAV. The average execution time of each UAV at each step is less than 0.035 ms, as shown in Fig. 9, demonstrating the proposed method can work in real time.

Lan *et al.* [2] adopted a similar idea with this article by designing the coordinated path-following control law in the coordination set $\mathcal{S}_1$, and the single-agent level control law in $\mathcal{S}_2$. However, the control law in [2] is designed for unicycles without considering constraints (2). The trajectories of the UAVs by employing the method in [2] are shown in Fig. 10, where the parameters of the UAVs' constraints and the coordination set, as well as the initial positions of the UAVs are set the same as in our settings. The control inputs v_i and ω_i are postprocessed to satisfy the fixed-wing UAVs' constraints. Since v_i obtained directly from the control law in [2] can be negative, when it is postprocessed to let $v_i = v_{\min}$, some UAVs (UAVs 2, 3, and 6) are getting further and further from the desired path. Besides, since the coordination set for fixed-wing UAVs is relatively small, the single-agent level control law in $\mathcal{S}_2$ should be properly designed to guarantee the UAVs enter the coordination set, which is not necessarily satisfied by the method in [2]. Thus, it fails to solve the coordinated path-following control problem for fixed-wing UAVs.

B. HIL Simulation

To further validate the proposed algorithm, an HIL simulation environment is constructed, which consists of four computers running the *X-Plane*[5] flight simulator, four *autopilots*, and a *ground control station*, as shown in Fig. 11. We use Ethernet networks for the communications among the three parts. The plane chosen in our HIL simulation is the *Great Planes PT-60 RC plane* [13], [17]. With all these facilities, we have conducted two typical HIL simulations, i.e., cyclic pursuit on a circle and multiple curved path following. The HIL simulations demonstrate the feasibility of the real-time onboard implementations of the proposed algorithms.

1) Cyclic Pursuit: In this setting, first, three UAVs are executing the coordinated path-following algorithm, and trying to follow the path while being distributed evenly on the orbit. After the system becomes stable, the fourth UAV joins. The orbit and the control parameters are set as the same as those in Section V-A.

During the control process, the measured inner-loop tracking error of the forward speed and the angular speed is 0.33 m/s and 0.01 rad/s, respectively. Though there exist inner-loop tracking errors, it can be seen from Fig. 12(a) and (b) that ρ_i and ψ_i corresponding to the four UAVs almost converge to 0, and the joining of the fourth UAV has no influence on the stability of the path-following control of the former three UAVs. The arc distances between UAVs are shown in Fig. 12(c). We can see that the arc distances can be steered to around the desired value whether there are three or four UAVs. We can also find that there are cyclic fluctuations in arc distances. The fluctuations are caused by two main reasons. The first reason is that our control law is based on the first-order system, with the acceleration period ignored in our model. The second reason is attributed to the establishment of the cyclic interaction topology in this scenario, in which each UAV has a preneighbor to follow. We have already shown that the proposed control law can stabilize the arc distances for the first-order UAV model in Fig. 7(c). Later, we will show in another example that with a tree interaction topology, the cyclic fluctuation can be eliminated or reduced. We also note that the fewer UAVs, the smaller fluctuations would

[5]The *X-Plane* flight simulator is favored by many researchers to test their flight control algorithms for its ultrarealistic flight simulation [13], [17].

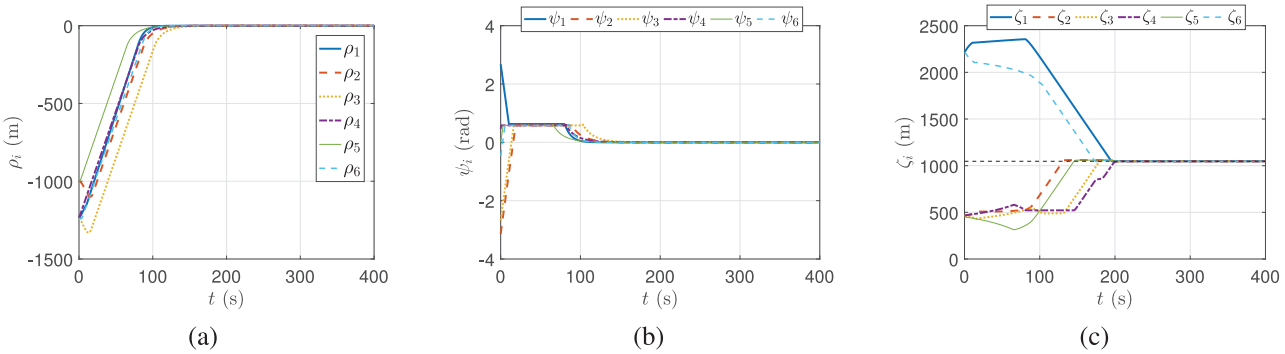

Fig. 7. Coordinated path-following performance in numerical simulation. (a) Each UAV's location difference ρ_i. (b) Each UAV's orientation difference ψ_i. (c) Arc distance ζ_i between every two adjacent UAVs.

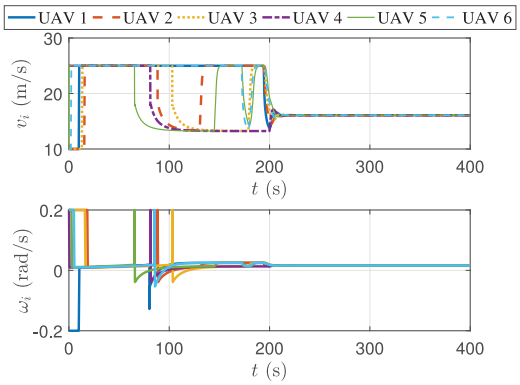

Fig. 8. Control inputs of each UAV.

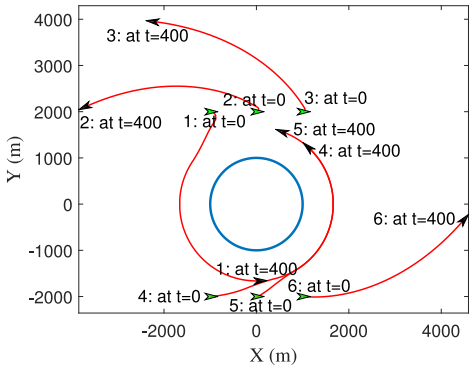

Fig. 10. Trajectories of six UAVs following a circle with the method in [2], while v_i and ω_i are constrained.

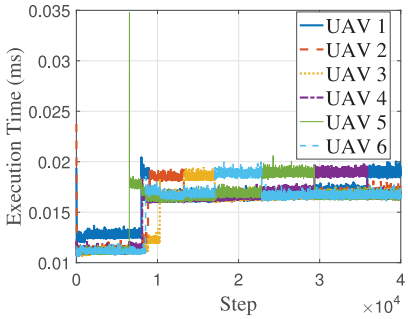

Fig. 9. Average execution time of each UAV at each step.

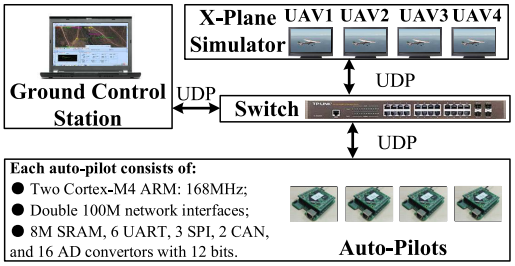

Fig. 11. HIL simulation environment.

be, as shown in Fig. 12(c), where the fluctuation for 3-UAV coordination is smaller than that for 4-UAV coordination.

2) Multipath Following: With a little bit of modification, we show our proposed hybrid control law can steer a fleet of UAVs to move on multiple paths and achieve a desired "in-line" formation pattern. In this case, each UAV has its own target path, and when one path is given, the other paths can be generated through the translation transformation of this path. Still, the interaction topology is not pre-established but formed when all the UAVs enter $\mathcal{S}_1$. In order to achieve an in-line formation pattern, we set $L = 0$, and $\chi(\cdot)$ is defined as $\chi(\zeta_i) = 0.475\zeta_i + v^r_{\min}$. We employ a cubic B-Spline curve [17] to obtain a continuous and nonconstant curvature path. We select seven points as shown in Table I to generate the cubic B-Spline for UAV 1 to follow. In Table I, the Lon and the Lat represent the longitude and latitude, respectively. Besides, we establish a north-east coordinate with the origin positioned at the first waypoint of UAV 1, such that all the UAVs' states can be represented in an xy-plane. The positions of the waypoints in this new coordinate are also provided in Table I.

The simulation results of the multipath following scenario are shown in Fig. 13. The path for UAV 1 is generated by B-spline, then by moving along the y-direction for 100, 200, and 300 m, we get the planned paths for UAV 2, UAV 3, and UAV 4, respectively, which are shown by the dashed curves in Fig. 13. We can see that all the UAVs fly along the planned paths while achieving the desired in-line formation pattern during the flight.

The arc distances between adjacent UAVs are shown in Fig. 14. Contrary to the cyclic pursuit case with a cyclic interaction topology, the interaction topology established in

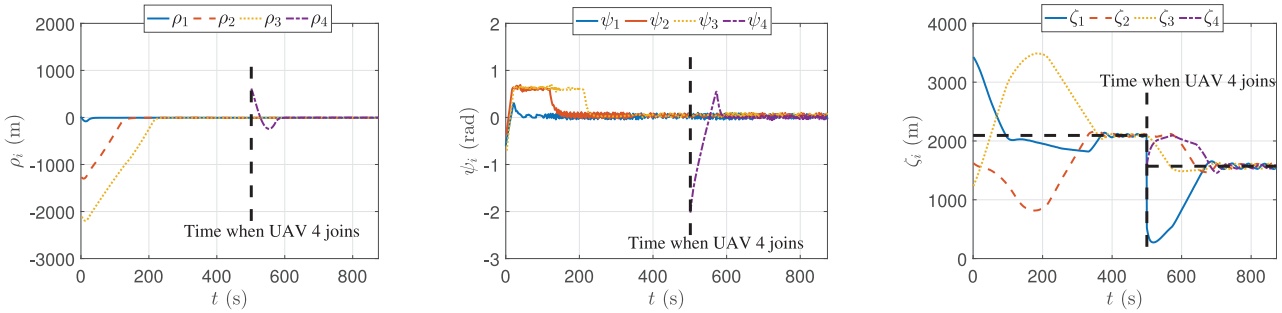

Fig. 12. Coordinated path-following performance in the HIL simulation of cyclic pursuit. (a) Each UAV's location difference ρ_i. (b) Each UAV's orientation difference ψ_i. (c) Arc distance ζ_i between every two adjacent UAVs.

TABLE I
POSITIONS OF WAYPOINTS

Waypoint	1	2	3	4	5	6	7
Lon/deg	113.2167	113.2371	113.2167	113.1963	113.2167	113.2371	113.2167
Lat/deg	28.2029	28.2209	28.2390	28.2570	28.2751	28.2931	28.3112
x/m	0	2006.43	4013.47	6019.83	8026.83	10033.19	12040.19
y/m	0	1996.54	0	-1997.26	0	1997.87	0

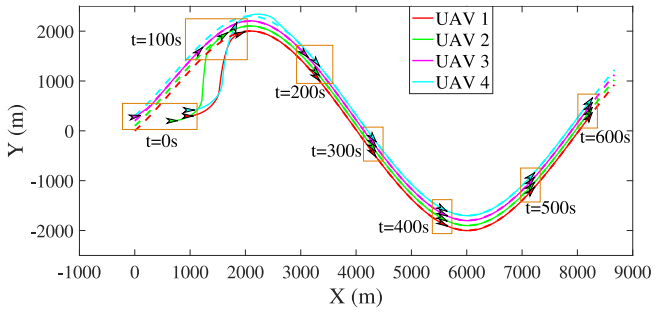

Fig. 13. Multipath following of four UAVs, while achieving the "in-line" formation pattern.

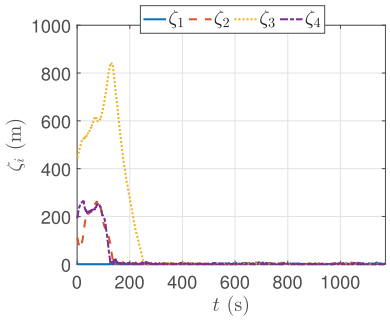

Fig. 14. Arc distance ζ_i between every two adjacent UAVs in the HIL simulation of multipath following.

this scenario is a tree, with UAV 1 as the global leader of the formation. We can see that the cyclic fluctuations are eliminated in Fig. 14.

VI. CONCLUSION

In this article, we have investigated the problem of steering a fleet of fixed-wing UAVs with speed constraints along any $\mathcal{C}^2$-smooth path with maximum curvature $\kappa_0 \leq \omega_{\max}/v_{\min}$, while achieving sequenced desired inter-UAV arc distances. We have proposed the hybrid control law based on the defined coordination set: for each UAV, if its path-following error is within this coordination set, then the UAV follows the path in a coordination manner with its preneighbor; otherwise, the UAV works at the single-agent level which individually controls the path-following error toward the coordination set. To handle the speed constraints from fixed-wing UAVs, we transform the parameter selection problem for the coordination set to an optimization problem, while satisfying the speed constraints of fixed-wing UAVs, as well as guaranteeing the convergence of both the path-following error and the coordination error. We have also calculated the admissible set for these two errors reducing to zero when the UAVs are executing our proposed control law. The algorithm is validated with both numerical and HIL simulation, respectively, demonstrating the effectiveness of the proposed approach.

The proposed approach can scale up to handle different velocity bounds for heterogeneous fixed-wing UAVs by designing different coordination sets, provided that all the UAVs have a common feasible speed. Future work includes extending the proposed approach to the three-dimensional case, considering communication delay, loss of communication, and optimization of the energy assumption, convergence rate, etc.

APPENDIX A
PROOF OF LEMMA 3

When ϕ_i is in the first quadrant, with (8), we have

$$\begin{aligned} 0 &\geq v_m(a\sin\psi_i + R_1\kappa_0\cos\psi_i) - R_1\omega_{\max} + R_1\alpha \\ &\geq v_m\left(a\sin\psi_i - R_1\frac{\kappa(p_i)\cos\psi_i}{1-\kappa(p_i)\rho_i}\right) - R_1\omega_{\max} + R_1\alpha. \end{aligned} \tag{31}$$

Thus, (4) is derived when $v_i \in [v_{\min}, v_m]$ and $\omega_i = -\omega_{\max}$.

When ϕ_i is in the second quadrant, with (9), we have

$$-\alpha \geq -\omega_{\max} + \frac{v_m\kappa_0}{1-\kappa_0 R_1} \geq -\omega_{\max} - \frac{v_m\kappa(p_i)\cos\psi_i}{1-\kappa(p_i)\rho_i}.$$

Thus, (5) is derived when $v_i \in [v_{\min}, v_m]$ and $\omega_i = -\omega_{\max}$.

Inequalities (6) and (7) can be concluded in the same way.

APPENDIX B
PROOF OF LEMMA 4

Denoting the speed that the ith UAV moves along the path as v_i^r, then $v_i^r = [(\cos\psi_i)/(1-\kappa(p_i)\rho_i)]v_i$. Let the jth UAV be the preneighbor of the ith UAV, and $\phi_i, \phi_j \in \mathcal{S}_1$, then $\dot{\zeta}_i = v_j^r - v_i^r$. Suppose initially $0 < \zeta_i(t_0) \le L-\delta_1$, where $0 < \delta_1 < L$, if (10) holds, we can choose $v_i \in [v_{\min}, v_m]$ and $v_j \in [v_{\min}, v_{\max}]$, such that $v_i^r = [1/(1-\kappa_0 R_1)]v_{\min}$, $v_j^r \ge [1/(1-\kappa_0 R_1)]v_{\min}$, then $\dot{\zeta}_i \ge 0$ holds for $t \ge t_0$, as a result, $\zeta_i > 0$ always holds, i.e., there exists a proper control law such that no overtaking occurs.

APPENDIX C
PROOF OF LEMMA 6

We take $\phi_i(t) \in \mathcal{S}_1^1$ as an example. If ω_i is not saturated in line 3, i.e., $\omega_i = \omega_d$, then the value of v_i will not be changed in RESETVALUE, since the left-hand side of inequality (4) becomes

$$\begin{aligned} & v_{i1}\left[a\sin\psi_i - R_1\frac{\kappa(p_i)\cos\psi_i}{1-\kappa(p_i)\rho_i}\right] + R_1\omega_i + R_1\alpha \\ &= av_{i1}\sin\psi_i - \frac{k_1R_1v_{i1}}{k_2}(k_1\rho_i + k_2\psi_i + k_3\sin\psi_i) \\ &\le av_{i1}\sin\psi_i - k_1R_1v_{i1}\psi_i \overset{(a)}{\le} 0. \end{aligned}$$

where inequality (a) is caused by $k_1R_1 \ge a$ and $0 < \psi_i < \pi/2$. Therefore, inequality (4) holds when $\omega_i = \omega_d$. As a result, v_i will not be changed in RESETVALUE.

Now suppose $\omega_i = \omega_{\max}$, which means $\omega_d \ge \omega_{\max}$, the left-hand side of inequality (4) becomes

$$\begin{aligned} & v_{i1}\left[a\sin\psi_i - R_1\frac{\kappa(p_i)\cos\psi_i}{1-\kappa(p_i)\rho_i}\right] + R_1\omega_{\max} + R_1\alpha \\ &\le v_{i1}\left[\frac{k_1R_1}{k_2}(k_1\rho_i + k_2\psi_i + k_3\sin\psi_i) - R_1\frac{\kappa(p_i)\cos\psi_i}{1-\kappa(p_i)\rho_i}\right] \\ &\quad + R_1\alpha + R_1\omega_{\max} = R_1(-\omega_d + \omega_{\max}) \le 0. \end{aligned}$$

Inequality (4) holds, implying that v_i will not be changed.

Finally, if $\omega_i = -\omega_{\max}$ and v_i is changed in RESETVALUE, then the returned value is

$$\begin{aligned} v_i &= \left[a\sin\psi_i - R_1\frac{\kappa(p_i)\cos\psi_i}{1-\kappa(p_i)\rho_i}\right]^{-1} R_1(\omega_{\max} - \alpha) \\ &\ge \frac{R_1(\omega_{\max} - \alpha)}{a\sin\psi_i + R_1\kappa_0\cos\psi_i} \overset{(b)}{\ge} v_m, \end{aligned}$$

where inequality (b) follows from (31). Clearly, $v_i < v_{i1}$; otherwise, inequality (4) will hold and v_i does not need to be changed. Thus, if $\phi_i \in \mathcal{S}_1^1$, and v_i is changed in RESETVALUE, then $v_m \le v_i < v_{i1}$.

Results for the other five subsets are deduced similarly.

REFERENCES

[1] X. Wang *et al.*, "Coordinated flight control of miniature fixed-wing UAV swarms: Methods and experiments," *Sci. China Inf. Sci.*, vol. 62, Sep. 2019, Art. no. 212204.

[2] Y. Lan, G. Yan, and Z. Lin, "Synthesis of distributed control of coordinated path following based on hybrid approach," *IEEE Trans. Autom. Control*, vol. 56, no. 5, pp. 1170–1175, May 2011.

[3] I. Kolmanovsky and N. H. McClamroch, "Developments in nonholonomic control problems," *IEEE Control Syst. Mag.*, vol. 15, no. 6, pp. 20–36, Dec. 1995.

[4] C. Samson, "Path following and time-varying feedback stabilization of a wheeled mobile robot," in *Proc. ICARCV*, 1992, p. 13.

[5] D. R. Nelson, D. B. Barber, T. W. Mclain, and R. W. Beard, "Vector field path following for miniature air vehicles," *IEEE Trans. Robot.*, vol. 23, no. 3, pp. 519–529, Jun. 2007.

[6] G. Ambrosino, M. Ariola, U. Ciniglio, F. Corraro, E. De Lellis, and A. Pironti, "Path generation and tracking in 3-D for UAVs," *IEEE Trans. Control Syst. Technol.*, vol. 17, no. 4, pp. 980–988, Jul. 2009.

[7] S. Lee, A. Cho, and C. Kee, "Integrated waypoint path generation and following of an unmanned aerial vehicle," *Aircraft Eng. Aerosp. Technol.*, vol. 82, no. 5, pp. 296–304, 2010.

[8] P. B. Sujit, S. Saripalli, and J. B. Sousa, "Unmanned aerial vehicle path following: A survey and analysis of algorithms for fixed-wing unmanned aerial vehicles," *IEEE Control Syst. Mag.*, vol. 34, no. 1, pp. 42–59, Feb. 2014.

[9] S. Park, J. Deyst, and J. P. How, "Performance and Lyapunov stability of a nonlinear path following guidance method," *J. Guid. Control Dyn.*, vol. 30, no. 6, pp. 1718–1728, 2007.

[10] N. Cho, Y. Kim, and S. Park, "Three-dimensional nonlinear differential geometric path-following guidance law," *J. Guid. Control Dyn.*, vol. 38, no. 12, pp. 2366–2385, 2015.

[11] I. Rhee, S. Park, and C.-K. Ryoo, "A tight path following algorithm of an UAS based on PID control," in *Proc. SICE Annu. Conf.*, 2010, pp. 1270–1273.

[12] Y. Q. Liang and Y. M. Jia, "Combined vector field approach for 2D and 3D arbitrary twice differentiable curved path following with constrained UAVs," *J. Intell. Robot. Syst.*, vol. 83, no. 1, pp. 133–160, 2016.

[13] S. Zhao, X. Wang, Z. Lin, D. Zhang, and L. Shen, "Integrating vector field approach and input-to-state stability curved path following for unmanned aerial vehicles," *IEEE Trans. Syst., Man, Cybern., Syst.*, vol. 50, no. 8, pp. 2897–2904, Aug. 2020.

[14] S. Jackson, J. Tisdale, M. Kamgarpour, B. Basso, and J. K. Hedrick, "Tracking controllers for small UAVs with wind disturbances: Theory and flight results," in *Proc. 47th IEEE Conf. Decis. Control*, 2008, pp. 564–569.

[15] M. Ahmed and K. Subbarao, "Nonlinear 3-D trajectory guidance for unmanned aerial vehicles," in *Proc. 11th Inter. Conf. Control Autom. Robot. Vis.*, 2010, pp. 1923–1927.

[16] C. Cao, N. Hovakimyan, V. V. Patel, I. Kaminer, and V. Dobrokhodov, "Stabilization of cascaded systems via L1 adaptive controller with application to a UAV path following problem and flight test results," in *Proc. Amer. Control Conf.*, 2007, pp. 1787–1792.

[17] S. Zhao, X. Wang, D. Zhang, and L. Shen, "Curved path following control for fixed-wing unmanned aerial vehicles with control constraint," *J. Intell. Robot. Syst.*, vol. 89, nos. 1–2, pp. 107–119, 2018.

[18] V. Roldao, R. Cunha, D. Cabecinhas, C. Silvestre, and P. Oliveira, "A leader-following trajectory generator with application to quadrotor formation flight," *Robot. Auton. Syst.*, vol. 62, no. 10, pp. 1597–1609, 2014.

[19] L. Liu, D. Wang, Z. Peng, and T. Li, "Modular adaptive control for LOS-based cooperative path maneuvering of multiple underactuated autonomous surface vehicles," *IEEE Trans. Syst., Man, Cybern., Syst.*, vol. 47, no. 7, pp. 1613–1624, Jul. 2017.

[20] H. Chen, X. Wang, L. Shen, and Y. Cong, "Formation flight of fixed-wing UAV swarms: A group-based hierarchical approach," *Chin. J. Aeronaut.*, to be published, doi: 10.1016/j.cja.2020.03.006.

[21] J. Ghommam, H. Mehrjerdi, M. Saad, and F. Mnif, "Formation path following control of unicycle-type mobile robots," *Robot. Auton. Syst.*, vol. 58, no. 5, pp. 727–736, 2010.

[22] Q. Li and Z. P. Jiang, "Pattern preserving path following of unicycle teams with communication delays," *Robot. Auton. Syst.*, vol. 60, no. 9, pp. 1149–1164, 2012.

[23] S. Zhao, X. Wang, H. Chen, and Y. Wang, "Cooperative path following control of fixed-wing unmanned aerial vehicles with collision avoidance," *J. Intell. Robot. Syst.*, vol. 100, pp. 1569–1581, Jun. 2020.

[24] G. Antonelli, F. Arrichiello, and S. Chiaverini, "Flocking for multi-robot systems via the null-space-based behavioral control," *Swarm Intell.*, vol. 4, no. 1, p. 37, 2010.

[25] J. Werfel, K. Petersen, and R. Nagpal, "Designing collective behavior in a termite-inspired robot construction team," *Science*, vol. 343, no. 6172, pp. 754–758, 2014.

[26] K.-K. Oh, M.-C. Park, and H.-S. Ahn, "A survey of multi-agent formation control," *Automatica*, vol. 53, pp. 424–440, Mar. 2015.

[27] X. Wang, Z. Zeng, and Y. Cong, "Multi-agent distributed coordination control: Developments and directions via graph viewpoint," *Neurocomputing*, vol. 199, pp. 204–218, Jul. 2016.
[28] D. B. Wilson, A. H. Goktogan, and S. Sukkarieh, "Vision-aided guidance and navigation for close formation flight," *J. Field Robot.*, vol. 33, no. 5, pp. 661–686, 2016.
[29] Z. Sun, H. G. de Marina, G. S. Seyboth, B. D. Anderson, and C. Yu, "Circular formation control of multiple unicycle-type agents with non-identical constant speeds," *IEEE Trans. Control Syst. Technol.*, vol. 27, no. 1, pp. 192–205, Jan. 2019.
[30] T. H. Chung, M. R. Clement, M. A. Day, K. D. Jones, D. Davis, and M. Jones, "Live-fly, large-scale field experimentation for large numbers of fixed-wing UAVs," in *Proc. IEEE Int. Conf. Robot. and Autom. (ICRA)*, 2016, pp. 1255–1262.
[31] V. Cichella *et al.*, "Safe coordinated maneuvering of teams of multirotor unmanned aerial vehicles: A cooperative control framework for multi-vehicle, time-critical missions," *IEEE Control Syst. Mag.*, vol. 36, no. 4, pp. 59–82, Aug. 2016.
[32] L. A. V. Reyes and H. G. Tanner, "Flocking, formation control, and path following for a group of mobile robots," *IEEE Trans. Control Syst. Technol.*, vol. 23, no. 4, pp. 1268–1282, Jul. 2015.
[33] E. Xargay *et al.*, "Time-critical cooperative path following of multiple unmanned aerial vehicles over time-varying networks," *J. Guid. Control Dyn.*, vol. 36, no. 2, pp. 499–516, 2013.
[34] Y. Wang, D. Wang, and S. Zhu, "Cooperative moving path following for multiple fixed-wing unmanned aerial vehicles with speed constraints," *Automatica*, vol. 100, pp. 82–89, Feb. 2019.
[35] R. W. Beard and T. W. McLain, *Small Unmanned Aircraft: Theory and Practice*. Princeton, NJ, USA: Princeton Univ. Press, 2012.
[36] F. A. Fontes, D. B. Fontes, and A. C. Caldeira, "Model predictive control of vehicle formations," in *Optimization and Cooperative Control Strategies*. New York, NY, USA: Springer, 2009, pp. 371–384.
[37] H. K. Khalil, *Nonlinear Systems*. Upper Saddle River, NJ, USA: Prentice-Hall, 2002.
[38] I. Barkana, "Defending the beauty of the invariance principle," *Int. J. Control*, vol. 87, no. 1, pp. 186–206, 2014.
[39] J. Yang, D. Yin, and L. Shen, "Reciprocal geometric conflict resolution on unmanned aerial vehicles by heading control," *J. Guid. Control Dyn.*, vol. 40, no. 10, pp. 2511–2523, 2017.

Hao Chen received the B.E., M.E., and Ph.D. degrees in control science and engineering from the National University of Defense Technology, Changsha, China, in 2013, 2015, and 2020, respectively.

He is currently a Lecturer with the College of Intelligence Science and Technology, National University of Defense Technology. He was a visiting student with the Technion—Israel Institute of Technology, Haifa, Israel, from 2017 to 2018. His research interests include coordinated control and graph theory.

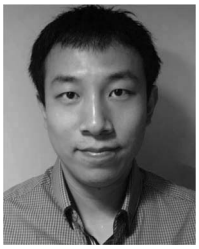

Yirui Cong (Member, IEEE) received the B.E. degree in automation from Northeastern University, Shenyang, China, in 2011, the M.E. degree in control science and engineering from the National University of Defense Technology, Changsha, China, in 2013, and the Ph.D. degree in the cross fields of communication theory and control theory from Australian National University, Canberra, ACT, Australia, in 2018.

He is currently an Associate Professor with the College of Intelligence Science and Technology, National University of Defense Technology. His research interests are in the fields of communication theory and control theory.

Xiangke Wang (Senior Member, IEEE) received the B.E., M.E., and Ph.D. degrees in control science and engineering from the National University of Defense Technology, Changsha, China, in 2004, 2006, and 2012, respectively.

Since 2012, he has been with the College of Intelligence Science and Technology, National University of Defense Technology, where he is currently a Professor. He was a visiting student with Australian National University, Canberra, ACT, Australia, from 2009 to 2011. His research interests include multiagent systems, nonlinear control, and unmanned aerial vehicles.

Xin Xu (Senior Member, IEEE) received the B.E. and Ph.D. degrees in control science and engineering from the National University of Defense Technology (NUDT), Changsha, China, in 1996 and 2002, respectively.

He was a Visiting Professor with Hong Kong Polytechnic University, Hong Kong; the University of Alberta, Edmonton, AB, Canada; the University of Guelph, Guelph, ON, Canada; and the University of Strathclyde, Glasgow, U.K. He is currently a Professor with the College of Intelligence Science and Technology, NUDT. He has coauthored four books. His research interests include reinforcement learning, approximate dynamic programming, machine learning, robotics, and autonomous vehicles.

Prof. Xu was a recipient of the Fork Ying Tong Youth Teacher Fund of China in 2008 and the Second Class National Natural Science Award of China in 2012. He is currently an Associate Editor of *Information Sciences*, *International Journal of Robotics and Automation*, and *Acta Automatica Sinica*. He was a Guest Editor of the *International Journal of Adaptive Control and Signal Processing* and the IEEE TRANSACTIONS ON SYSTEMS, MAN, AND CYBERNETICS: SYSTEMS. He is a member of the IEEE Computational Intelligence Society Technical Committee on Approximate Dynamic Programming and Reinforcement Learning and the IEEE Robotics and Automation Society Technical Committee on Robot Learning.

Lincheng Shen received the B.E., M.E., and Ph.D. degrees in automatic control from the National University of Defense Technology, Changsha, China, in 1986, 1989, and 1994, respectively.

He is currently a Professor with the College of Intelligence Science and Technology, National University of Defense Technology, where he serves as the Dean of the Graduate School. His research interests include unmanned aerial vehicles, swarm robotics, and artificial intelligence.

Prof. Shen has initiated and organized several workshops and symposia, including the International Workshop on Bionic Engineering in 2012 and the Chinese Automation Congress in 2013. He has been serving as an Editorial Board Member of the *Journal of Bionic Engineering* since 2007.